NASA TECHNICAL NOTE

NASA TN D-3959

NASA TN D-3959

N67-24475
(ACCESSION NUMBER)
(THRU)
247
(PAGES)
(CODE)
01
(NASA CR OR TMX OR AD NUMBER)
(CATEGORY)
FACILITY FORM 602

ANALYTICAL STUDIES OF ASPECT RATIO AND CURVATURE VARIATIONS FOR AXIAL-FLOW-COMPRESSOR-INLET STAGES UNDER HIGH LOADING

by Ronald J. Steinke and James E. Crouse

Lewis Research Center

Cleveland, Ohio

NATIONAL AERONAUTICS AND SPACE ADMINISTRATION • WASHINGTON, D. C. • MAY 1967

NASA TN D-3959

ANALYTICAL STUDIES OF ASPECT RATIO AND CURVATURE VARIATIONS FOR AXIAL-FLOW-COMPRESSOR-INLET STAGES UNDER HIGH LOADING

By Ronald J. Steinke and James E. Crouse

Lewis Research Center
Cleveland, Ohio

NATIONAL AERONAUTICS AND SPACE ADMINISTRATION

For sale by the Clearinghouse for Federal Scientific and Technical Information
Springfield, Virginia 22151 – CFSTI price $3.00

ANALYTICAL STUDIES OF ASPECT RATIO AND CURVATURE VARIATIONS FOR AXIAL-FLOW-COMPRESSOR-INLET STAGES UNDER HIGH LOADING

by Ronald J. Steinke and James E. Crouse

Lewis Research Center

SUMMARY

An analytical study of the performance changes of axial-flow compressors with increased aspect ratio and loading was made. The computer program used to make the calculations included the streamline curvature and the radial gradient of the combined profile and shock losses in the radial equation of motion. A radially constant energy addition was used throughout the studies.

Compressor-inlet stages with aspect ratios of 3.0 to 6.0 for the case of zero tip curvature and with aspect ratios of 3.0 to 9.0 for the case of high tip curvature were investigated. For an aspect ratio of 8.0, calculations were also carried out at a reduced tip curvature and at a reduced loading.

Generally, the studies indicate that, with a proper choice of compressor passage geometry, curvature effects could be employed to control high-pressure-loss gradients to some extent and to reduced the possibility of tip-region stalling. Specifically, comparisons of the results of the zero-tip-curvature case with the high-tip-curvature case showed that tip-curvature effects reduced tip-region rotor-inlet Mach numbers and permitted a significant increase in aspect ratio while maintaining subsonic meridional velocities. Also, tip curvature caused rotor diffusion factors to decrease at the blade ends.

Although the studies illustrate that substantial flow redistributions occur at high aspect ratios because of curvature effects, the studies do not indicate any basic limit on aspect ratio for acceptable design point performance.

INTRODUCTION

Propulsion systems for advanced aircraft, such as the supersonic transport or

V/STOL type, require compact compressors of light weight and high performance. These compressor requirements imply high flow per unit of frontal area and a high pressure ratio per unit of axial length. High flow capacity is achieved in axial-flow compressors designed for high, subsonic, axial inlet velocities and low hub-tip radius ratios. A high pressure ratio per unit of axial length can be achieved by using high work input per stage and by using short axial length per stage of high blade aspect ratio.

Suitable flow rates and pressure ratios have been obtained individually in previous studies. High flow has been demonstrated experimentally by single-stage studies such as in reference 1 where a corrected flow of 37.6 pounds per second per square foot of frontal area was obtained for a hub-tip ratio of 0.35. A pressure ratio of 2.0 for a single rotor with a hub-tip ratio of 0.7 was reported in reference 2. It must be recognized that some compromise of flow capacity and stage pressure ratio must be made based on factors such as tip relative Mach number, rotor-hub energy addition, and blade flow blockage effects.

Although high-aspect-ratio blading is effective in increasing pressure ratio per unit of axial length, it has inherent aerodynamic and mechanical design problems. Reference 3 showed the necessity of including curvature and entropy terms in the radial equilibrium equation used in high-aspect-ratio design procedure. References 4 and 5 have shown that increases in aspect ratio have resulted in a decreased range of operation between choke and stall limits, but no loss in peak efficiency. The maximum aspect ratio used in these experiments, however, was only 2.1.

To obtain high-stage pressure ratios and high flow rates at favorable efficiencies, refinements in compressor aerodynamic design and analysis procedures are required to match the blade rows properly. At high aspect ratios in particular, these refinements include the necessity to calculate curvature effects and the radial distribution of losses accurately, because they both have a strong influence on the radial distribution of through-flow velocity.

In the analysis presented herein, various flow parameters are calculated for axial-flow-compressor-inlet stages of different annular geometries over a range of blade aspect ratios above 3.0. The objectives of this study are to evaluate the effect of aspect-ratio-curvature variations and radial distributions of pressure losses on flow parameters such as meridional velocity, diffusion factor, etc. and to determine whether any basic limit of aspect ratio exists in order to maintain acceptable design point performance. Off-design performance and the mechanical problems of high-aspect-ratio blading are not considered in this investigation.

COMPUTATIONAL PROCEDURE

The main features of the computer program are first discussed and then related to

the method of analysis used to investigate variations in aspect ratio, curvature, and loading.

Computer Program

A streamline analysis program was used in the calculations to study effects of the variation of input data on compressor flow parameters and performance. The important characteristics of the computer program are listed as follows:

(1) Flow parameters and performance quantities are calculated along radial lines only at axial stations exterior to blade rows.

(2) Steady, nonviscous, axisymmetric flow is assumed.

(3) Losses must be calculated external to the program and their effects included by the appropriate total pressure P and total temperature T relation. (Symbols are defined in appendix A.)

(4) The radial position of the calculated output quantities can be determined in terms of specified weight-flow intervals.

(5) Streamline curvature is determined by using a beam-fit technique to describe streamline shape between axial stations.

(6) Along radial lines, the radial-equilibrium equation, which includes streamline-curvature terms and radial-loss gradients, is satisfied simultaneously with the flow-continuity equation.

(7) Meridional velocities V_m greater than 97 percent of sonic and less than 1.0 foot per second are not permitted. The program limits V_m to this range to prevent continuity iteration instabilities.

The streamline curvature computed by the beam fit will remain constant only at the hub and tip where diameter variations with axial position are fixed program inputs. At all other radial positions, streamline curvature will vary with the computed flow properties. The computer program uses an iteration process to locate the streamlines so that the flow equations are satisfied with curvature terms included.

Method of Analysis

The computational procedure is governed by the limitations the computer program places on the meridional velocity V_m. The truncating of V_m at 97 percent of sonic, in effect, sets an upper limit on the aspect ratio which can be investigated for a given compressor-stage geometry, since the maximum value of V_m increases with aspect ratio because of increased curvature effects. At a radial position where the lower limit

on V_m of 1.0 foot per second is reached, the flow parameters are not computed accurately. The distribution of flow parameters throughout the corresponding weight-flow interval can thus only be approximated. Low V_m values near 1 foot per second, however, are always well into a local compressor-stall region; therefore it is insignificant that flow parameters are not computed accurately in this region.

Rotor- and stator-outlet radial total-pressure distributions must be specified as computer program input data. These required total-pressure distributions were obtained by subtracting the total-pressure losses from the ideal total pressure. For fixed compressor geometry (including aspect ratio) and inlet conditions, rotor and stator pressure losses are functions of radial position, blade-section diffusion factor, relative inlet Mach number, etc. A strong dependence of pressure loss on radial position gives rise to high radial gradients of total pressure that alter the flow conditions. Since pressure losses are dependent on computed flow parameters, a lengthy pressure-loss iteration procedure was required external to the program to match input pressure losses with output data. Appendix B discusses the details of the pressure-loss iteration process and loss correlations which were used. Pressure losses were taken as the summation of profile loss and shock loss. The variation of blade profile loss with blade loading and radial position used in this analysis were based on experimental data taken from reference 6 and are shown graphically in figure 5 (see appendix B). Of primary significance is the rapid increase of rotor profile pressure loss with radius in the mean-to-tip blade region which was used in the loss correlations. For a given high level of diffusion factor, rotor profile losses are generally several times higher at the tip than at the mean or hub.

The analyses were divided into four major phases according to the relative amounts of curvature at the hub and tip and the energy addition across the rotor. Table I lists the

TABLE I. - COMPRESSOR CURVATURE CHARACTERISTICS, ASPECT RATIO RANGE, AND ENERGY ADDITION FOR EACH PHASE OF ANALYSIS

Phase of analysis	Geometry	Curvature		Aspect ratios	Radially constant energy addition at rotor outlet, ft^2/sec
		Hub	Tip		
I	Figure 2(a)	Very high	Zero	3.0, 4.0, 5.0, 6.0	702
II	Figure 3(a)	High	High	3.0, 4.0, 6.0, 8.0, 9.0	702
III	Figure 4(a)	Low	Low	8.0	702
IV	Figure 3(a)	High	High	8.0	526

TABLE II. - BASIC INPUT DATA WHICH REMAINED CONSTANT FOR ALL FOUR PHASES OF ANALYSIS

Constant quantity for all four phases of analysis	Assumed constant value
Weight flow, w, lb/sec	153.1
Nominal rotor-inlet average axial velocity, $\overline{V}_{z,1}$, ft/sec	650
Rotor-inlet tip speed, $U_{1,t}$, ft/sec	1400
Rotor-inlet total pressure, P_1, lb/ft^2	2116
Rotor-inlet total temperature, T_1, ^oR	518.7
Rotor-inlet rV_θ for all radii, ft^2/sec	0
Stator-outlet rV_θ for all radii, ft^2/sec	0
Rotor-inlet tip radius, $r_{1,t}$, ft	1.250
Rotor-inlet hub radius, $r_{1,h}$, ft	0.625
Tip-blade solidity, σ_t	1.25

compressor curvature characteristics, aspect-ratio range, and level of radially constant energy addition rV_θ used for each phase. The levels of energy addition chosen were large enough to obtain high-stage total-pressure ratios. In conjunction with high-aspect-ratio blading, these high-stage pressure ratios reflect the desired characteristics for lightweight compressors. Basic input data, which were held constant for all four phases, are given in table II. The nominal average axial velocity at the rotor inlet $\overline{V}_{z,1}$ given in table II, represents the velocity which would be obtained if streamline-curvature effects are ignored. A typical velocity diagram at the rotor outlet is shown in figure 1.

Aspect ratio was defined as the ratio of rotor-inlet blade height to blade axial length. Changes in aspect ratio were accomplished by allowing inversely proportional changes in the blade axial dimension and space between blade rows. For a given aspect ratio, all compressor-inlet stages studied have the same rotor-stator axial dimensions and spacing. The compressor stages used in phases I, II, and IV have the same annulus areas at all corresponding axial positions. In phase III, annulus areas were increased upstream of the rotor and decreased downstream of the rotor in order to permit reduction in hub and tip curvature. The blade solidity was chosen to be inversely proportional to radial distance throughout the studies. For all stages, the tangential velocity V_θ was taken to be zero at the rotor inlet and stator outlet.

In phase I, a compressor stage with zero tip curvature and very high hub curvature was studied for aspect ratios of 3.0 to 6.0. The work input term rV_θ was chosen to remain constant (702 ft^2/sec) with radius at the rotor outlet. From this value, rotor- and stator-outlet total temperature and pressure corresponding to zero pressure losses were calculated and used as the program for the initial pressure-loss iteration. Particular attention is given to the behavior of flow parameters in the rotor-tip and stator-hub region. These are critical regions where variations in diffusion factor and Mach number will exert a strong influence on profile and shock losses. Radial distributions of total-pressure ratio, meridional velocity, diffusion factor, inlet Mach number, and stage adiabatic efficiency are calculated.

Phase II studies used a compressor stage with high tip curvature and less hub curva-

ature than used in phase I. Aspect ratios of 3.0 to 9.0 were investigated in the same manner and for the same level of work input as in phase I.

Phase III studies used a compressor stage of 8.0 aspect ratio with lower hub and tip curvature than used in phase II. The loading level and investigation procedure used in phase II were also used in the phase III studies.

In phase IV, the 8.0-aspect-ratio compressor stage of phase II was studied for a 25-percent reduction in the work input term rV_θ. Otherwise, the same method of investigation was used as in phase II.

RESULTS AND DISCUSSION

The results of the four major phases of the study are discussed individually in this section. Particular attention is given to the behavior of flow parameters in the rotor-tip and stator-hub regions. These are critical regions where variations in diffusion factor and Mach number will exert a strong influence on profile and shock losses. Appropriate comparisons of the results of phase studies are made.

Phase I - Studies of Zero-Tip-Curvature and Very-High-Hub-Curvature Compressor Stages

Results are presented for aspect ratios of 3.0 to 6.0 for the zero-tip-curvature (constant o.d.) and very-high-hub-curvature compressor stages incorporating the pressure-loss iteration process described in appendix B. The compressor geometry is shown in figure 2(a), which illustrates the large increase of hub curvature with increase of aspect ratio. The flow parameters of both the initial and final pressure-loss iterations are shown in figures 2(b) to (*l*).

Radial distributions of total-pressure ratio. - The total-pressure-ratio distributions are shown in figures 2(b) and (c) for the rotor and stator outlets. For all aspect ratios, there is a general decrease of total pressure with increased radius. As aspect ratio is increased, the overall mass-averaged pressure ratios decrease (table III). A very rapid drop in total pressure occurred in the tip region especially for aspect ratios 3.0, 4.0, and 5.0. These compressor stages appear to be stalling in this tip region which will be explained in greater detail in the discussions of the other flow parameters. Dashed lines are used in the figures in the 10-percent weight-flow interval nearest the tip where total-pressure values are approximate.

TABLE III. - OVERALL MASS-AVERAGED QUANTITIES

FOR EACH PHASE OF ANALYSIS

Phase of analysis	Aspect ratio	Overall mass-averaged quantity		
		Rotor outlet to inlet total-pressure ratio, P_2/P_1	Stator outlet to rotor inlet total-pressure ratio, P_4/P_1	Stage adiabatic efficiency, η_{ad}
I	3.0	1.91	1.81	0.72
	4.0	1.89	1.80	.71
	5.0	1.86	1.77	.69
	6.0	1.78	1.69	.63
II	3.0	1.89	1.78	0.70
	4.0	1.88	1.77	.70
	6.0	1.88	1.77	.70
	8.0	1.86	1.75	.69
	9.0	1.84	1.74	.67
III	8.0	1.85	1.76	0.69
IV	8.0	1.63	1.59	0.75

For the zero-tip-curvature compressor stages, increasing the aspect ratio proves to be detrimental to the total-pressure ratio. However, a design with a work gradient or with a less severe loss distribution could improve the total-pressure ratio.

Radial distributions of meridional velocity. - The meridional velocity distributions shown in figures 2(d-1) to (g-2) for the rotor and stator inlets and outlets illustrate the strong influence that changes in aspect ratio and radial variations of losses have on V_m. The V_m distributions for the initial iteration with zero pressure losses give the effects of curvature changes independent of loss gradients, and the V_m distributions for the final iteration of pressure losses include the effect of the loss gradients.

Initial iteration - zero pressure losses: In general, for zero or constant pressure losses, increasing the aspect ratio has two major effects on the streamlines: (1) the absolute value of the streamline curvature is increased, and (2) the streamline slope is increased. Increases in the absolute value of streamline curvature will cause the gradient of the radial distribution of meridional velocity to increase. Increased slope introduces higher radial velocities and, hence, higher meridional velocity. For the constant-outside-diameter compressor geometry (fig. 2(a)), the magnitude of both streamline slope and curvature would decrease with increased radius. Also, the sign of streamline curvatures would be expected to change from rotor inlet to outlet, since hub curvature was chosen to be concave toward the flow passage at the rotor inlet and convex toward the flow

passage downstream of the rotor.

At the rotor inlet (fig. 2(d-1)), the effects of changes in streamline slope and curvature on meridional velocity V_m are quite evident for changes in aspect ratio. The V_m's increase with aspect ratio for a fixed radial position, and they also increase with radius for any given aspect ratio. The increases in the gradient of the meridional velocity with increases in aspect ratio are large in the hub region where curvature effects are strong. At the tip, the V_m gradients approach zero since curvature effects vanish because of the constant outside diameter. For an aspect ratio of 6.0, high streamline curvature and slope caused V_m to become supersonic at radial positions in excess of approximately 85 percent of the tip radius. The computer program truncates V_m at 97 percent of sonic and, thus, the entire plot of V_m is only an approximation. A dashed curve for V_m is shown where V_m is transonic.

At the rotor outlet (fig. 2(e-1)) and the stator inlet and outlet (figs. 2(f-1) and (g-1)), the meridional velocities V_m decrease with increased radius for a given aspect ratio for the initial iteration. This behavior of V_m for a fixed aspect ratio occurred because the compressor geometry (fig. 2(a)) is such that hub curvature downstream of the rotor has the opposite sign as compared with hub curvature at the rotor inlet. At the axial stations downstream of the rotor, the V_m behavior for aspect ratio changes is similar to that at the rotor inlet. The V_m values increase with aspect ratio in the high-curvature hub regions and the V_m radial gradients are small in the low-curvature tip regions.

Final iteration of pressure losses: The magnitude and gradient of the pressure losses across the rotor were sufficient to cause substantial alterations in the meridional velocity distributions at the rotor inlet (fig. 2(d-2)). The V_m values have decreased in the tip region and increased in the midblade region. A region of transonic meridional velocity is still present, however, at the rotor inlet for an aspect ratio of 6.0. When the pressure loss is considered, the meridional velocities at the rotor outlet (fig. 2(e-2)) and the stator inlet and outlet (figs. 2(f-2) and (g-2)) drop off very rapidly in the tip regions and increase in the hub and midblade regions. Near-sonic V_m were encountered, especially at the stator outlet, again for an aspect ratio of 6.0. For aspect ratios 3.0, 4.0, and 5.0, the V_m at the tip were reduced to the computer program limit of 1.0 foot per second. Dashed lines are shown in the figures for regions where meridional velocities are approximate.

It may be concluded, for the compressor geometry chosen, that supersonic V_m can be expected at the rotor inlet at an aspect ratio between 5.0 and 6.0. Therefore, an upper limit to aspect ratio exists if sonic meridional velocities are to be avoided. Supersonic meridional velocities may be undesirable because of shock losses and difficulty in obtaining adequate design control.

The rapid decrease of V_m toward zero in the tip regions of stations downstream of the rotor (figs. 2(e-2), (f-2), and (g-2)) for the low aspect ratios occurred because of the

high-loss gradients associated with the high level of radially constant work input rV_θ which was used. These low tip V_m's could be raised by a design for more work input in regions of high loss, but it may be necessary to reduce the average work level in order to permit increased work locally. Thus, the tip-region stalling which occurred for low aspect ratios is not considered to be a basic limitation.

Radial distributions of diffusion factor. - Diffusion factor distributions for the rotor and stator are shown in figures 2(h-1) to (i-2). (The dashed portion of the curves near the tip are approximate.) Their values are high at most radii since rV_θ was high. The diffusion factors could be reduced by increasing blade solidity; however, the trends are of primary interest in this study.

Initial iteration - zero pressure losses: Several trends are worth nothing:

(1) At the tip, the rotor and stator diffusion factors increase with an increasing aspect ratio.

(2) At the hub, the diffusion factors decrease with increasing aspect ratio.

(3) For a given aspect ratio, maximum rotor diffusion factors occur in the midblade region.

Similar trends would be expected for a radially constant pressure loss. The trends seem to indicate that, in regions of high curvature (i. e., the hub region) for the given compressor geometry, an increase in aspect ratio which intensifies curvature effects causes a decrease in diffusion factor. Also, for a given aspect ratio, the rapid decrease of rotor diffusion factor in the hub region is primarily due to the combination of concave upward curvature which would decrease V_m at the inlet and concave downward curvature which would increase V_m at the outlet.

Final iteration of pressure losses: The gradient of pressure losses caused the following changes:

(1) Both rotor and stator diffusion factors in the hub and midblade regions decreased from their values of the initial iteration.

(2) Tip region diffusion factors, especially for the stator, increased sharply.

The behavior of the diffusion factor at the rotor tip and stator hub is critical because of the influence on losses. Hence, for the particular constant-outside-diameter annulus geometry chosen, increases in aspect ratio have no apparent benefit for the rotor tip, but they are advantageous for the stator hub.

Radial distributions of inlet Mach number. - Radial distributions of rotor-inlet relative Mach number and stator-inlet absolute Mach number are shown in figures 2(j-1) to (k-2) for the initial and final pressure-loss iterations. Generally, for all aspect ratios, the inlet Mach number increases with radius at the rotor inlet and decreases with increasing radius at the stator inlet. Also, the inlet Mach number increases with aspect ratio for nearly all radii. Therefore, a high aspect ratio would be expected to result in

high shock losses and would be deleterious for the given constant-outside-diameter compressor stages.

Radial distributions of stage adiabatic efficiency. - The stage adiabatic efficiency distributions are shown in figure 2(*l*) for the final total-pressure-loss iteration. The very rapid decrease of adiabatic efficiency in the tip region for all aspect ratios was caused by the high profile losses associated with high rotor- tip- and stator-tip-region diffusion factors and the high shock losses associated with high rotor-tip-region relative inlet Mach numbers. Adiabatic efficiency decreased slightly in the hub region for all aspect ratios because of increases in the stator diffusion factor and high stator-inlet absolute Mach numbers. The general increase of rotor- and stator-inlet Mach numbers with high aspect ratios contributed to the decrease of adiabatic efficiency in the midblade region.

As shown in table III, the adiabatic efficiency for the overall mass-averaged state consistently decreased as the aspect ratio increased. Thus, the constant-outside-diameter compressor geometry shown in figure 2(a) would perform poorly for high-aspect-ratio blading at the given high-loading level. The rapid decrease of tip-region efficiencies especially for the low aspect ratios could be alleviated by alterations in the loading level and/or loading distribution. A work gradient, for example, could be used to control possible tip-region stalling and thus, help to improve low-aspect-ratio tip-region performance.

Phase II - Studies of High-Hub- and Tip-Curvature Compressor Stages

The high hub- and tip-curvature compressor-stage geometry is shown in figure 3(a). At the rotor inlet, the absolute value of the streamline slope at the tip is half as large as at the hub. Results for aspect ratios of 3.0 to 9.0 are shown in figure 3 for both the initial and final pressure-loss iterations. For the final total-pressure-loss iteration, the lower limit on V_m was reached at the tip for aspect ratios 3.0 and 4.0. Dashed lines are used in the figures to denote approximate values. With pressure losses, stalling would probably occur near the tip for aspect ratios 3.0 and 4.0.

Radial distributions of total-pressure ratio. - The total-pressure-ratio distributions shown in figures 3(b) and (c) exhibit a general decrease of total pressure with radius similar to the previous phase I constant-outside-diameter studies. In the phase II studies, however, the tip curvature reduces tip-region losses and total-pressure increases with aspect ratio at the tip. This decrease of tip-region pressure losses alleviated somewhat the drop in the overall mass-averaged pressure ratios of the phase I studies (see table III). Thus, tip curvature is concluded to be beneficial to maintaining favorable overall pressure ratios for high-aspect-ratio blading.

Radial distributions of meridional velocity. - The meridional velocity distributions

are shown in figures 3(d-1) to (g-2) for the initial and final pressure-loss iterations.

Initial iteration - zero pressure losses: Without losses, the V_m behavior can be related to curvature. For a given axial distance, the sign of tip curvature is opposite to that of hub curvature. Therefore, the slope of the V_m distribution at the hub is opposite to that at the tip. Also, somewhere between the hub and tip there exists a region of very small curvature where V_m will have a maximum or minimum value. The important differences from the zero-tip-curvature phase I studies are as follows:

(1) At the rotor inlet, V_m decreases with increased radius in the tip region.

(2) At the rotor outlet and stator inlet, V_m increases toward the tip.

(3) At the stator outlet, tip-curvature effects are small and the V_m distributions resemble those of the constant-outside-diameter phase I studies.

Final iteration of pressure losses: The meridional velocity distributions illustrate substantial changes due to pressure losses. The V_m at the rotor outlet and stator inlet and outlet increases over values for zero pressure losses in the hub region, and for the low aspect ratios, V_m decreases rapidly with radius in the tip regions. The advantages of having tip curvature are evident especially for the high-aspect-ratio cases where curvature effects are strong. At the rotor inlet, the decrease of V_m in the tip region permits the aspect ratio to be at least 9.0 before transonic flow is reached instead of between 5.0 and 6.0 without tip curvature. At the further downstream axial positions, the V_m values remain more nearly uniform for the high aspect ratios, and the possibility of stalling is reduced.

Tip curvature is thus concluded to help in the prevention of both transonic V_m at the rotor inlet and stalling conditions further downstream.

Radial distributions of diffusion factor. - The diffusion factor distributions shown in figures 3(h-1) to (i-2) demonstrate the effects of tip curvature and radial variation of losses.

Initial iteration - zero pressure losses: Rotor-tip diffusion factors decrease when the aspect ratio increases, rather than increasing with the aspect ratio as occurred in the constant-outside-diameter phase I studies. Also, the maximum diffusion factor in the mean region increases to a higher level. Little change occurs in the stator diffusion factor distributions without pressure losses between phases I and II.

Final iteration of pressure losses: Tip-curvature effects are strong enough for the high aspect ratios to maintain low rotor-tip diffusion factors with losses included. Generally, stator diffusion factors tend to decrease when the aspect ratio is increased at the tip and at the hub for high aspect ratio. Therefore, based on diffusion factor, high aspect ratio is advantageous at the rotor tip and has some benefits to stator-hub performance for the particular compressor geometry chosen.

Radial distributions of inlet Mach number. - Distributions of rotor-inlet relative Mach numbers and stator-inlet absolute Mach numbers are shown in figures 3(j-1) to (k-2)

for the initial and final pressure-loss iterations. At the rotor inlet, Mach number increases with aspect ratio and radius except in the tip region where curvature effects reverse the trend. The given tip curvature would thus be beneficial for controlling tip-region shock losses as compared with phase I. The stator-inlet Mach number generally decreases with radius except near the tip where curvature effects cause it to increase with radius for high aspect ratio. Aspect-ratio variations and tip curvature have little effect on the stator-hub Mach number.

Radial distributions of stage adiabatic efficiency. - The stage adiabatic efficiency distributions shown in figure 3(*l*) resemble those of the constant-outside-diameter phase I studies. However, tip curvature has now caused tip-region efficiencies to increase with aspect ratio. As shown in table III (p. 7), the overall mass-averaged stage adiabatic efficiencies do not drop as rapidly with increased aspect ratio as they did in the constant-outside-diameter phase I studies. In conclusion, tip curvature is beneficial for maintaining relatively high overall efficiencies at high aspect ratio.

For the low aspect ratios, the rapid decrease of tip-region efficiency and tip-region stalling could be alleviated by using a low work level or a work gradient in a similar manner as was previously discussed in the phase I studies. Thus, the poor performance of the low-aspect-ratio blading could be improved.

Phase III - Studies of 8.0-Aspect-Ratio Compressor Stage at Reduced Curvature

Studies were performed at an aspect ratio of 8.0 in which the hub and tip curvature were reduced from those used for the high-curvature compressor stage of the phase II studies. The low hub- and tip-curvature compressor-stage geometry which was used is shown in figure 4(a) with the high-curvature compressor stage (fig. 2(a)) indicated by dashed lines for comparison. The results for the final pressure-loss iteration are shown in figures 4(b) to (*l*) and are compared with the results of the previous (phase II) 8.0-aspect-ratio high-curvature compressor study. (The results of phase IV studies which will be discussed on p. 14 are also shown in the figures.)

Radial distributions of total-pressure ratio. - The rotor- and stator-outlet total-pressure distributions (figs. 4(b) and (c)) indicate that the low hub- and tip-curvature compressor stage produced effects in the tip regions which are similar to those previously obtained by curvature reduction due to aspect-ratio reduction. Specifically, tip-region total pressure decreased when tip curvature decreased. However, hub-region total pressure also decreased for the low-curvature compressor; this pressure reduction did not occur in the previous aspect-ratio-variation studies (phase II). Little change occurred in the mass-averaged total-pressure ratios given in table III.

By comparing the changes in the rotor and stator total-pressure distributions due to

aspect-ratio reduction (figs. 3(b) and (c)) to the changes due to hub- and tip-curvature reduction (figs. 4(b) and (c)), it can be predicted that lowering the aspect ratio to somewhere between 8.0 and 6.0 would have essentially the same effect on tip-region total pressures as would be obtained by using the low-curvature compressor stage.

Radial distributions of meridional velocity. - The effect of a reduction in hub and tip curvature is first evident at the rotor inlet (fig. 4(d)) where low curvature caused the meridional velocity to increase at the blade ends. At all the downstream locations (figs. 4(e) to (g)), the highest values of V_m occur in the midblade regions. For high curvature, the downstream V_m's tend to peak at the hub.

Comparisons with the meridional velocity distributions for the aspect-ratio phase II studies (figs. 3(d-2), (e-2), (f-2), and (g-2)) show that similar tip-region changes in the magnitude and slope of V_m at the rotor inlet and outlet can be obtained by lowering the aspect ratio as those produced for the low-curvature compressor stage. Also, at the stator-inlet- and stator-outlet-tip regions, the changes in slope are similar, but the magnitude of V_m has increased for the low-curvature compressor stage because of the smaller annulus areas.

Radial distributions of diffusion factor. - Rotor-hub-region, rotor-tip-region, and stator-hub-region diffusion factors (figs. 4(h) and (i)) increased for the low-curvature compressor stage. However, in the stator-tip region the diffusion factor decreased because of the previously discussed meridional velocity changes for the reduction in hub and tip curvature. Similar increases in rotor-tip and stator-hub diffusion factors occurred in the phase II studies when the aspect ratio was reduced (figs. 3(h-2) and 3(i-2)).

Radial distributions of inlet Mach number. - The inlet-Mach-number distributions (figs. 4(j) and (k)) for the low-curvature compressor stage, when compared with those for the high-curvature compressor stage, substantiate the influence of curvature effects on Mach number which were previously predicted by aspect-ratio variation (figs. 3(j-2) and (k-2)). Generally, it can be stated that, for the compressor geometries chosen, an increase in hub and tip curvature will cause the rotor-inlet relative Mach number (and associated shock losses) to rise in the midblade region and drop or remain about constant at the hub and tip. For the stator inlet, increases in hub and tip curvature, whether obtained by changes in passage shape or by increasing the aspect ratio, result in similar changes in the slope of the absolute-Mach-number curve. But the magnitude of the absolute Mach number is influenced by the reduction in annulus area for the low-curvature compressor stage and, hence, is not directly comparable to the phase II aspect-ratio studies.

In conclusion, for reduced Mach number and shock losses in the rotor-tip region, it appears that curvature is beneficial whether obtained by changes in passage shape or by increasing the aspect ratio.

Radial distributions of stage adiabatic efficiency. - The efficiency distributions

(fig. 3(l)) show that tip-region efficiency has decreased for the low-curvature compressor stage. Similar tip-region efficiency drops occurred for the phase II studies with low aspect ratios (fig. 3(l)). The overall mass-averaged efficiencies, however, remained about the same.

Phase IV - Studies of 8.0-Aspect-Ratio Compressor Stage at Reduced Loading

In the first three phases of the study, the work addition was at a level where the efficiencies indicated from present loss correlations are lower than desired. In this fourth phase of the study, rV_θ was reduced 25 percent to bring the work near the current level where a higher efficiency is indicated. The high hub- and tip-curvature compressor-stage geometry shown in figure 3(a) was used with an aspect ratio of 8.0. The results for the final pressure-loss iteration are shown in figures 4(b) to (l) and are compared with the results of the previous (phase II) 8.0-aspect-ratio high-curvature compressor study.

Radial distributions of total-pressure ratio. - The total-pressure-ratio curves (figs. 4(b) and (c)) demonstrate the overall drop of total pressure for the reduced rV_θ. Of more importance, it is noted that the absolute value of the slope of the rotor-outlet pressure curve has decreased, which indicates a decrease in rotor-tip-region pressure losses. Also, for the stator outlet, hub-region pressure losses have been reduced. The overall mass-averaged total-pressure ratios are given in table III.

Radial distributions of meridional velocity. - Little change in the meridional velocity distribution at the rotor inlet (fig. 4(d)) occurred with the reduced rV_θ as would be expected since the aspect ratio remained constant and, hence, curvature effects remained similar. At the rotor outlet and stator inlet (figs. 4(e) and (f)), the reduced rV_θ produced lower hub region V_m and higher tip region V_m. The relatively low V_m's for the rotor-outlet- and stator-inlet-hub regions are caused by the changes in the radial-loss gradients discussed in the previous section. At the stator outlet, the specification of zero rV_θ caused lower static pressures and densities for the reduced loading, and the V_m values have thus increased across the entire blade span.

The reduction in rV_θ has increased the V_m values in the tip region downstream of the rotor and would, hence, be beneficial to eliminating tip-region stalling.

Radial distributions of diffusion factor. - The distributions of rotor and stator diffusion factors (figs. 4(h) and (i)) show that the shape of the curves has remained similar for the reduced rV_θ as compared with the previous phase II study. The magnitudes of the diffusion factors have decreased for all radial positions especially at the rotor tip and stator hub. Therefore, rotor and stator profile losses will be substantially lower for the reduced rV_θ.

Radial distributions of inlet Mach number. - Little change occurred in the rotor-inlet relative Mach number (fig. 4(j)) with reduced rV_θ. However, stator-inlet absolute Mach number (fig. 4(k)) has decreased in the hub region primarily because the reduced tangential velocity V_θ resulted in a lower stator-inlet absolute velocity. Stator-hub-region shock losses would therefore be reduced.

Radial distributions of stage adiabatic efficiency. - Stage adiabatic efficiencies (fig. 4(*l*)) are higher for the reduced rV_θ study especially at the hub and tip. This increase in efficiency occurred primarily because of reduced rotor and stator diffusion factors; this condition caused losses to decrease more rapidly than energy input. Overall mass-averaged efficiencies are given in table III.

CONCLUDING REMARKS

The analytical studies showed that the effect of streamline curvature becomes larger and consequently more influential in establishing flow distributions as the aspect ratio is increased. Proper use of these effects may help counteract undesirable local loss distribution effects; however, they generally cannot compensate for a persistent loss gradient across the annulus. The results of this study imply that, even for the lower energy addition, it is difficult to maintain desirable distributions of stage outlet velocity and pressure through successive stages of a multistage compressor. It appears that to make high-aspect-ratio compressors perform well the loss gradients and curvature effects will probably have to be accurately accounted for and properly balanced with energy-addition gradients.

Some specific observations of the studies conducted were as follows:

(1) Radial gradients of pressure losses have effects on radial equilibrium in combination with those of curvature. The high-loss gradients caused meridional velocities downstream of the rotor to increase at the hub and decrease at the tip causing possible tip-region stalling for the constant-outside-diameter stages and the low-aspect-ratio cases with tip curvature. Low-loss gradients would tend to alleviate the tip stalling.

(2) The meridional velocity distribution is less distorted when casing curvature is used to balance hub-curvature effects. Tip-region-curvature effects can be used to allow a significant increase in aspect ratio while subsonic meridional velocities are maintained.

(3) Increases in the aspect ratio have the greatest influence in regions of high curvature. When casing curvature is concave toward the flow passage at the rotor inlet and convex further downstream, flow redistribution causes the rotor diffusion factor to decrease at the blade tip where profile losses are most severe.

(4) Flow redistributions, due to high-curvature effects, influence inlet Mach number distributions and, thus, the associated shock losses. For the compressor stages con-

sidered, rotor-inlet relative Mach number dropped at the blade ends but increased in the midblade region.

(5) Similar changes in the behavior of tip-region flow parameters and stage performance resulted from curvature reductions whether because of alterations in passage shape or because of low aspect ratios.

(6) For a constant wheel speed, a reduction in loading from a high level resulted in a decrease in pressure losses, especially near the tip and hub, and an increase in overall adiabatic efficiency. The outlet velocity distributions were also more uniform.

In conclusion, the results of these studies do not indicate any basic limit on aspect ratio other than possible supersonic meridional velocities for acceptable design point performance. It should be noted, however, that off-design performance and mechanical design problems may limit the maximum usable aspect ratio. Furthermore, profile losses were calculated by using a correlation based on experiments conducted on low-aspect-ratio blading below 3.0. The high axial pressure gradients associated with higher aspect-ratio blading could require refinements in the profile loss correlation that was used in order to predict performance accurately.

Lewis Research Center,
National Aeronautics and Space Administration,
Cleveland, Ohio, November 14, 1966,
720-03-01-48-22.

APPENDIX A

SYMBOLS

C_p	specific heat at constant pressure, Btu/(lb)(^oR)
D	diffusion factor (see eqs. (B2) and (B17))
g_c	acceleration due to gravity, 32.17 ft/sec^2
J	mechanical equivalent of heat, 778.2 ft-lb/Btu
M	Mach number
M_T	ratio of outlet element wheel speed to inlet relative stagnation velocity of sound
$\overline{M}$	average Mach number (see eqs. (B8) and (B23))
P	total pressure, lb/ft^2
(PBH)	percent of blade height from tip (see eqs. (B4) and (B19))
R	gas constant, 53.35 ft-lb/(lb)(^oR)
r	radius, ft
T	total temperature, ^oR
(TPLP)	total-pressure-loss parameter (see eqs. (B3) and (B18))
U	rotor speed, ft/sec
V	velocity, ft/sec
w	weight flow, lb/sec
z	coordinate along rotational axis, ft
β	angle between flow velocity and axial direction, deg
γ	ratio of specific heats
η_{ad}	stage adiabatic efficiency
$\Delta\nu$	amount of supersonic turning, deg
σ	solidity, ratio of chord to spacing
$\overline{\omega}$	total-pressure-loss coefficient

Subscripts:

h	hub
id	ideal
m	meridional
Pr	profile
R	rotor
r	radial direction
S	stator
Sh	shock
Su	suction surface

t tip

z axial direction

θ tangential direction

1 rotor inlet

2 rotor outlet

3 stator inlet

4 stator outlet

Superscript:

' relative to rotor

APPENDIX B

PRESSURE-LOSS ITERATION PROCESS

The pressure-loss iteration process required to match profile and shock losses to computer program output flow and blade loading parameters is discussed herein. For each iteration, a new set of loading parameters and pressure losses are calculated based on the velocity distributions of the previous iteration. For the initial iteration, a radial total-pressure-loss distribution must be assumed. The studies in this report assumed zero pressure losses for the initial iteration. Reasonable convergence of the iteration process (within a few percent of total pressure) occurred after four iterations.

Profile losses are obtained by using an extension of the correlation of pressure losses to diffusion factor and radial distance found in chaper VII of reference 6. Shock losses are related to relative inlet Mach number and supersonic turning as suggested in reference 7. Details of the procedure used to calculated rotor and stator pressure losses are now discussed.

Rotor Total-Pressure-Loss Calculation

The rotor blades are assumed to have a constant chord and, hence, the rotor solidity ratio is inversely proportional to radius. Furthermore, assuming a tip solidity of 1.25 results in

$$\sigma_R = \frac{1.25\, r_{1,t}}{r_1} \tag{B1}$$

With this assumed solidity variation, the rotor diffusion factor is obtained from

$$D_R = 1 - \frac{V_2'}{V_1'} + \frac{r_2 V_{\theta,2} - r_1 V_{\theta,1}}{(r_1 + r_2)\sigma_R V_1'} \tag{B2}$$

where the required velocities are obtained from the previous iteration. The rotor total-pressure-loss parameter is calculated from the empirical curve fit of loss data:

$$(TPLP)_R = 0.004 + 0.0639(D_R + 0.1)^{2.91} + 0.228 D_R^{2.02}\left[1 - \frac{(PBH)_R}{100}\right]^{3.77} \tag{B3}$$

where the percent of blade height from the rotor tip is given by

$$(PBH)_R = \frac{r_{2,t} - r_2}{r_{2,t} - r_{2,h}} (100) \tag{B4}$$

Equation (B3) is plotted in figure 5 and is based on the correlation presented in reference 6. For a given value of rotor diffusion factor, pressure losses in the tip region are substantially higher than at the hub. Finally, the rotor profile loss coefficient is obtained from

$$\bar{\omega}'_{Pr} = \frac{2\sigma_R (TPLP)_R}{\cos \beta'_2} \tag{B5a}$$

for all $\beta'_2 \leq 45^\circ$. Experimental data for an axial-flow-pump rotor (ref. 8) indicate that the $\bar{\omega}'_{Pr}$ given by equation (B5a) are too large for high β'_2. Therefore, $\bar{\omega}'_{Pr}$ was calculated from

$$\bar{\omega}'_{Pr} = 2\sqrt{2}\, \sigma_R (TPLP)_R \left[1 - \frac{\pi}{4} + \frac{\pi}{180} \beta'_2\right] \tag{B5b}$$

for all $\beta'_2 > 45^\circ$. For constant σ_R and $(TPLP)_R$, equation (B5b) gives $\bar{\omega}'_{Pr}$ as a linear function of β'_2 with the same slope as would be obtained from equation (B5a) at $\beta'_2 = 45^\circ$. Using equation (B5b) to calculate $\bar{\omega}'_{Pr}$ at high β'_2 eliminates the physically unrealistic high-loss coefficients given by equation (B5a) as β'_2 approaches 90°.

At all radial positions where the rotor-inlet relative Mach number M'_1 is greater than or equal to one, shock losses are accounted for as follows. Along the suction surface of the blade, supersonic turning is assumed to occur by means of a Prandtl-Meyer expansion as suggested in reference 7. The amount of supersonic turning is assumed to be directly proportional to total turning and inversely proportional to solidity. Furthermore, when assuming supersonic turning to be equal to half of total turning at the tip, the proportionality constant can be evaluated. The resulting equation is

$$\Delta\nu' = \frac{0.625(\beta'_1 - \beta'_2)}{\sigma_R} \tag{B6}$$

Using equation (B6) for supersonic turning eliminates the need to know the blade geometry in order to calculate $\Delta\nu'$ and, thus, simplifies the calculations. The peak suction-

surface Mach number is then obtained from

$$M'_{Su} = 1.095 + 0.03395\,\Delta\nu' + 1.086(M'_1 - 1.00)^{1.372} \tag{B7}$$

Equation (B7) is an approximation to the Prandtl-Meyer expansion and is plotted in figure 6 together with the exact solution. The approximate and exact solutions agree very well for inlet Mach numbers 1.0 to 1.4 except for a small region where M'_1 and $\Delta\nu'$ are low. The approximate solution was used because it permits M'_{Su} to be calculated directly, which cannot be done with the exact Prandtl-Meyer relation.

Shock losses are calculated based on the normal shock loss that would occur for a Mach number which is the average of the relative inlet and peak suction-surface Mach numbers. That is, for

$$\overline{M}' = \frac{M'_1 + M'_{Su}}{2} \tag{B8}$$

the shock-loss coefficient becomes

$$\overline{\omega}'_{Sh} = \frac{1 - \left[\dfrac{(\gamma + 1)(\overline{M}')^2}{(\gamma - 1)(\overline{M}')^2 + 2}\right]^{\gamma/\gamma-1}\left[\dfrac{\gamma + 1}{2\gamma(\overline{M}')^2 - (\gamma - 1)}\right]^{1/\gamma-1}}{1 - \left[1 + \dfrac{\gamma - 1}{2}(M'_1)^2\right]^{-\gamma/\gamma-1}} \tag{B9}$$

If the relative inlet Mach number is less than one, shock losses are accounted for as follows. A pseudopeak suction-surface Mach number M'_{Su} is calculated from equation (B7) by assuming that M'_1 is equal to one (i.e., the last term of eq. (B7) is set equal to zero). Then an average Mach number $\overline{M}'$ is computed from equation (B8) by using the pseudo M'_{Su} and the actual M'_1, which is less than one. If $\overline{M}'$ is greater than or equal to one, the shock-loss coefficient $\overline{\omega}'_{Sh}$ is obtained from equation (B9) by assuming a M'_1 of one. For $\overline{M}'$ less than one, shocks are assumed not to exist and $\overline{\omega}'_{Sh}$ is set equal to zero.

The total-pressure-loss coefficient is obtained by adding the profile-loss coefficient (eq. (B5)) to the shock-loss coefficient (eq. (B9)); that is,

$$\overline{\omega}' = \overline{\omega}'_{Pr} + \overline{\omega}'_{Sh} \tag{B10}$$

Then, with the equations in reference 6, the relative total-pressure ratio becomes

$$\frac{P_2'}{P_1'} = \left(\frac{P_2'}{P_1'}\right)_{id} - \bar{\omega}' \left[1 - \left(1 + \frac{\gamma - 1}{2}(M_1')^2\right)\right]^{-\gamma/\gamma - 1} \tag{B11}$$

where

$$\left(\frac{P_2'}{P_1'}\right)_{id} = \left\{1 + \frac{\gamma - 1}{2} M_T^2 \left[1 - \left(\frac{r_1}{r_2}\right)^2\right]\right\}^{\gamma/\gamma - 1} \tag{B12}$$

and

$$M_T = U_2 \left\{\gamma R g_c \left[T_1 + \frac{(V_1')^2 - (V_1)^2}{2C_p g_c J}\right]\right\}^{-0.5} \tag{B13}$$

Finally, the new total-pressure ratio is calculated from

$$\left(\frac{P_2}{P_1}\right) = \frac{\left(\frac{P_2'}{P_1'}\right)}{\left(\frac{P_2'}{P_1'}\right)_{id}} \left(\frac{T_2}{T_1}\right)^{\gamma/\gamma - 1} \tag{B14}$$

where the total-temperature ratio (T_2/T_1) is obtained from Euler's turbine equation when rV_θ is the basic assumed quantity:

$$\frac{T_2}{T_1} = 1 + \frac{U_2 V_{\theta,2} - U_1 V_{\theta,1}}{g_c J C_p T_1} \tag{B15}$$

The new refined outlet total pressures are calculated at eleven streamlines radially spaced at 10-percent weight-flow intervals and used as computer program inputs of the next iteration.

Stator Total-Pressure-Loss Calculation

The calculation procedure and equations for the stator losses are similar to those used for the rotor losses. The equations will be discussed only as necessary to clarify the differences between the rotor and stator loss calculation procedures.

Stator solidity and diffusion factor are obtained from

$$\sigma_S = \frac{1.25 r_{3,t}}{r_3} \tag{B16}$$

and

$$D_S = 1 - \frac{V_4}{V_3} + \frac{r_3 V_{\theta,3} - r_4 V_{\theta,4}}{(r_3 + r_4)\sigma_S V_3} \tag{B17}$$

The stator total-pressure-loss parameter and the percent of blade height from the stator tip are calculated from

$$(TPLP)_S = 0.004 + 0.0639(D_S + 0.1)^{2.91} + 0.057 D_S^{2.02}\left[1 - \frac{(PBH)_S}{100}\right]^{3.77} \tag{B18}$$

and

$$(PBH)_S = \frac{r_4 - r_{4,h}}{r_{4,t} - r_{4,h}}(100) \tag{B19}$$

Equation (B18) is plotted in figure 7 and differs from equation (B3) (fig. 5) only by a 75-percent reduction in the constant factor of the last term. The stator profile-loss coefficient is then obtained from

$$\overline{\omega}_{Pr} = \frac{2\sigma_S (TPLP)_S}{\cos \beta_4} \tag{B20}$$

Since β_4 is normally not greater than 45°, an additional equation for high values of β_4 was not required for the stators.

At radial positions where the stator-inlet Mach number M_3 is greater than or equal

to one, the shock-loss calculations are as follows:

For supersonic turning along the suction surface:

$$\Delta\nu = \frac{0.625(\beta_3 - \beta_4)}{\sigma_S} \tag{B21}$$

For peak suction-surface Mach number:

$$M_{Su} = 1.095 + 0.03395\,\Delta\nu + 1.086(M_3 - 1.00)^{1.372} \tag{B22}$$

For average Mach number:

$$\overline{M} = \frac{M_3 + M_{Su}}{2} \tag{B23}$$

For the stator shock-loss coefficient:

$$\overline{\omega}_{Sh} = \frac{1 - \left[\frac{(\gamma + 1)(\overline{M})^2}{(\gamma - 1)(\overline{M})^2 + 2}\right]^{\gamma/\gamma-1}\left[\frac{\gamma + 1}{2\gamma(\overline{M})^2 - (\gamma - 1)}\right]^{1/\gamma-1}}{1 - \left[1 + \frac{\gamma - 1}{2}(M_3)^2\right]^{-\gamma/\gamma-1}} \tag{B24}$$

For stator-inlet Mach numbers M_3 less than one, shock losses are accounted for in an analogous manner as was done for the rotor that was discussed previously (see Rotor Total-Pressure-Loss Calculation, p. 19).

The stator total-pressure-loss coefficient is obtained from

$$\overline{\omega} = \overline{\omega}_{Pr} + \overline{\omega}_{Sh} \tag{B25}$$

Across the stator the ideal relative total-pressure ratio and the total-temperature ratio are both one. Therefore, the new stator total-pressure ratio becomes

$$\frac{P_4}{P_3} = 1 - \overline{\omega}\left[1 - \left(1 + \frac{\gamma - 1}{2}(M_3)^2\right)^{-\gamma/\gamma-1}\right] \tag{B26}$$

where P_3 is assumed equal to P_2, the previously calculated total pressure at the rotor outlet.

Stator-outlet total pressures are calculated for the same eleven radially spaced streamlines as was done for the rotor.

REFERENCES

1. Cullom, Richard R.; Montgomery, John C.; and Yasaki, Paul T.: Experimental Performance of a 0.35 Hub-Tip Radius Ratio Transonic Axial-Flow-Compressor Stage Designed for 40 Pounds per Second per Unit Frontal Area. NACA RM E58D04a, 1958.

2. Klapproth, John F.; Jacklitch, John J. Jr.; and Tysl, Edward R.: Design and Performance of a 1400-Foot-per-Second-Tip-Speed Supersonic Compressor Rotor. NACA RM E55A27, 1955.

3. Carter, Anthony F.; and Novak, Richard A.: Computed Aspect Ratio - Curvature Effects Upon the Performance of a High-Pressure-Ratio Single-Stage Compressor. Paper No. 65-WA/GTP-12, ASME, Nov. 1965.

4. Kussoy, Marvin I.; and Bachkin, Daniel: Comparison of Performance of Two Aerodynamically Similar 14-Inch Diameter Single-Stage Compressor Rotors of Different Chord Length. NACA RM E57I03, 1958.

5. Sievers, Gilbert K.; Geye, Richard P.; and Lucas, James G.: Preliminary Analysis of Over-All Performance of an Eight-Stage Axial-Flow Research Compressor With Two Long-Chord Transonic Inlet Stages. NACA RM E57H14, 1958.

6. Robbins, William H.; Jackson, Robert J.; and Lieblein, Seymour: Blade-Element Flow in Annular Cascades. Aerodynamic Design of Axial-Flow Compressors, Irving A. Johnsen and Robert O. Bullock, eds. NASA SP-36, 1965, pp. 227-254.

7. Schwenk, Francis C.; Lewis, George W.; and Hartmann, Melvin J.: A Preliminary Analysis of the Magnitude of Shock Losses in Transonic Compressors. NACA RM E57A30, 1957.

8. Crouse, James E.; and Sandercock, Donald M.: Blade-Element Performance of 0.7 Hub-Tip Radius Ratio Axial-Flow-Pump Rotor with Tip Diffusion Factor of 0.43. NASA TN D-2481, 1964.

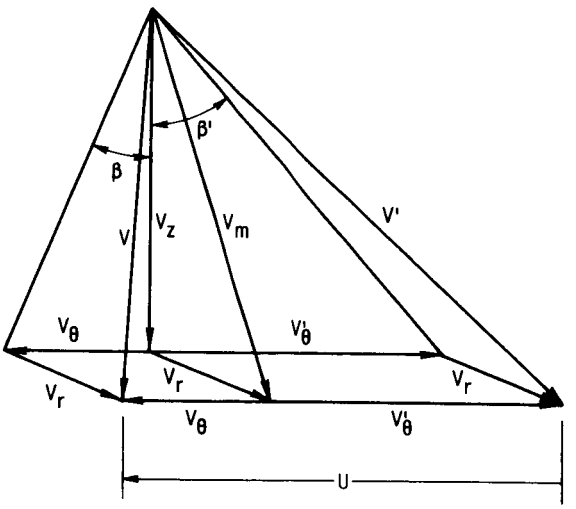

Figure 1. - Velocity diagram at rotor outlet.

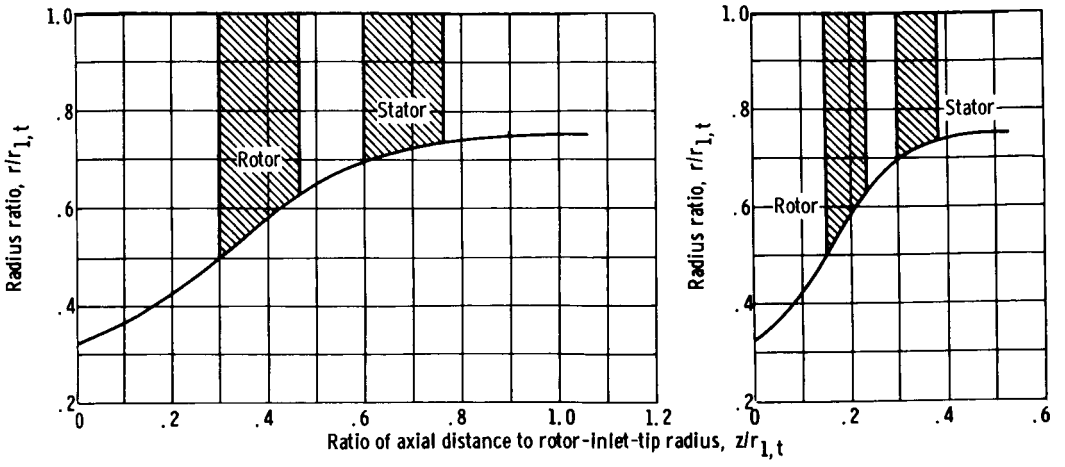

(a-1) Aspect ratio, 3.0.

(a-2) Aspect ratio, 6.0.

(a) Typical geometry of compressor stages.

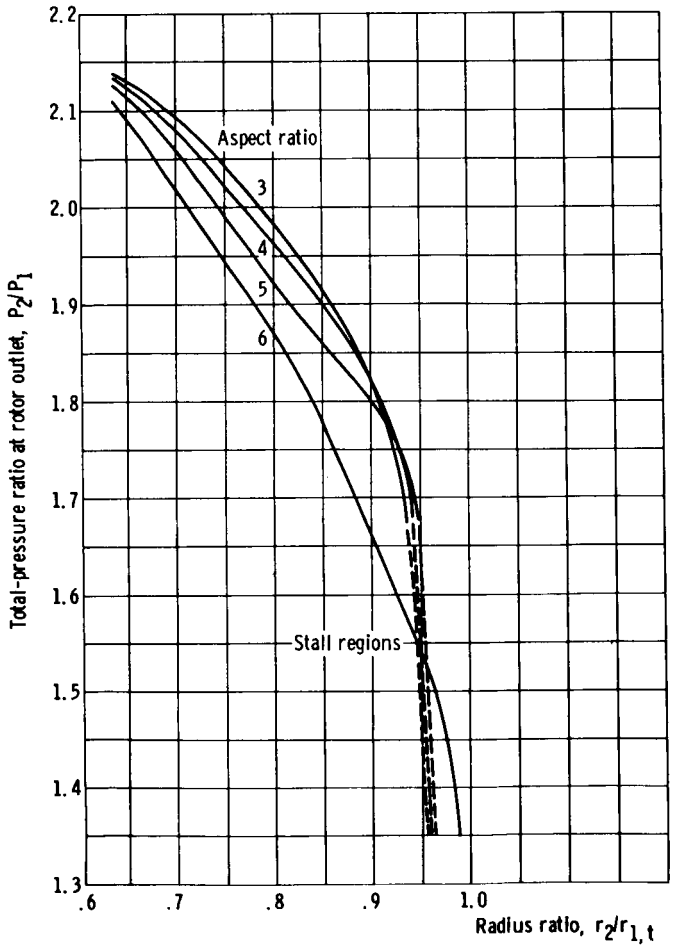

(b) Radial distributions of total pressure ratio at rotor outlet for final iteration of pressure losses.

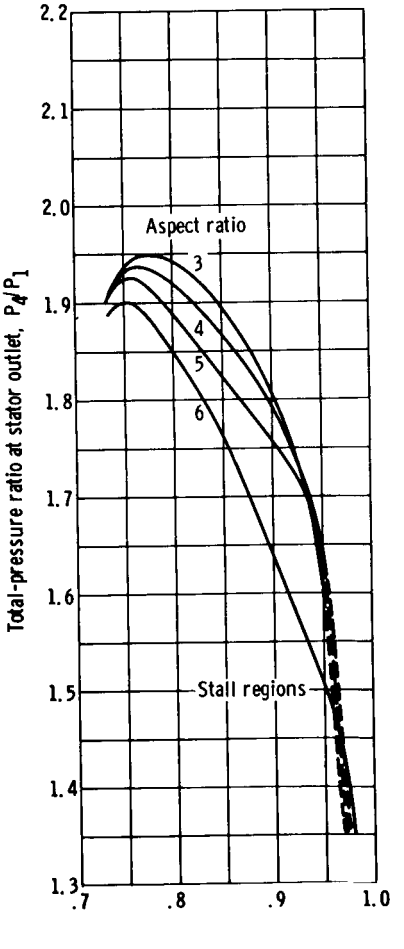

(c) Radial distributions of total pressure ratio at stator outlet for final iteration of pressure losses.

Figure 2. - Phase I studies of zero-tip-curvature and very-high-hub-curvature compressor stages for aspect ratios of 3.0 to 6.0.

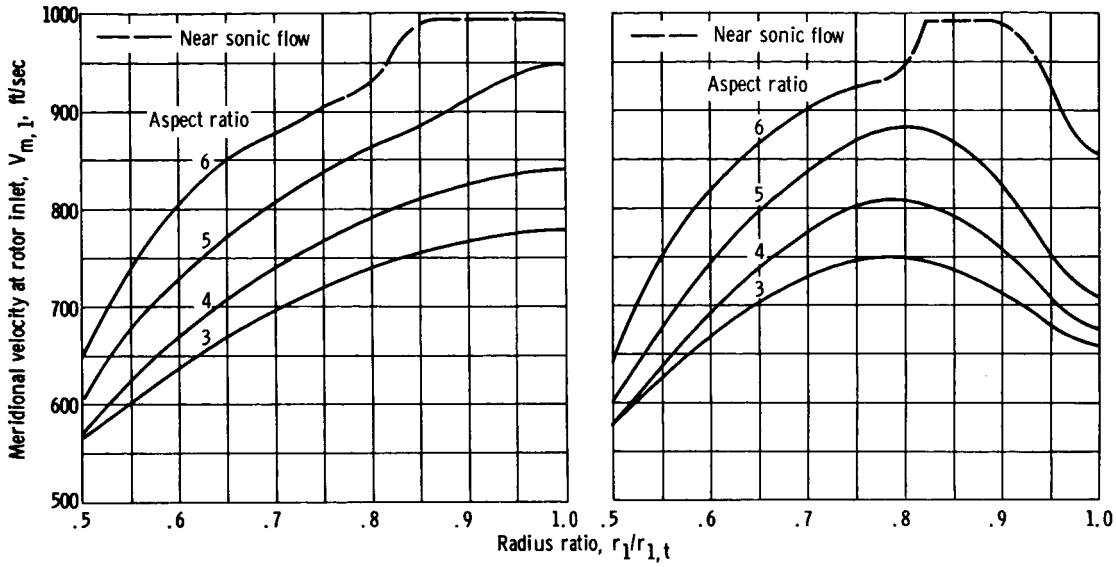

(d-1) Initial iteration - zero pressure losses. (d-2) Final iteration of pressure losses.

(d) Radial distribution of meridional velocity at rotor inlet.

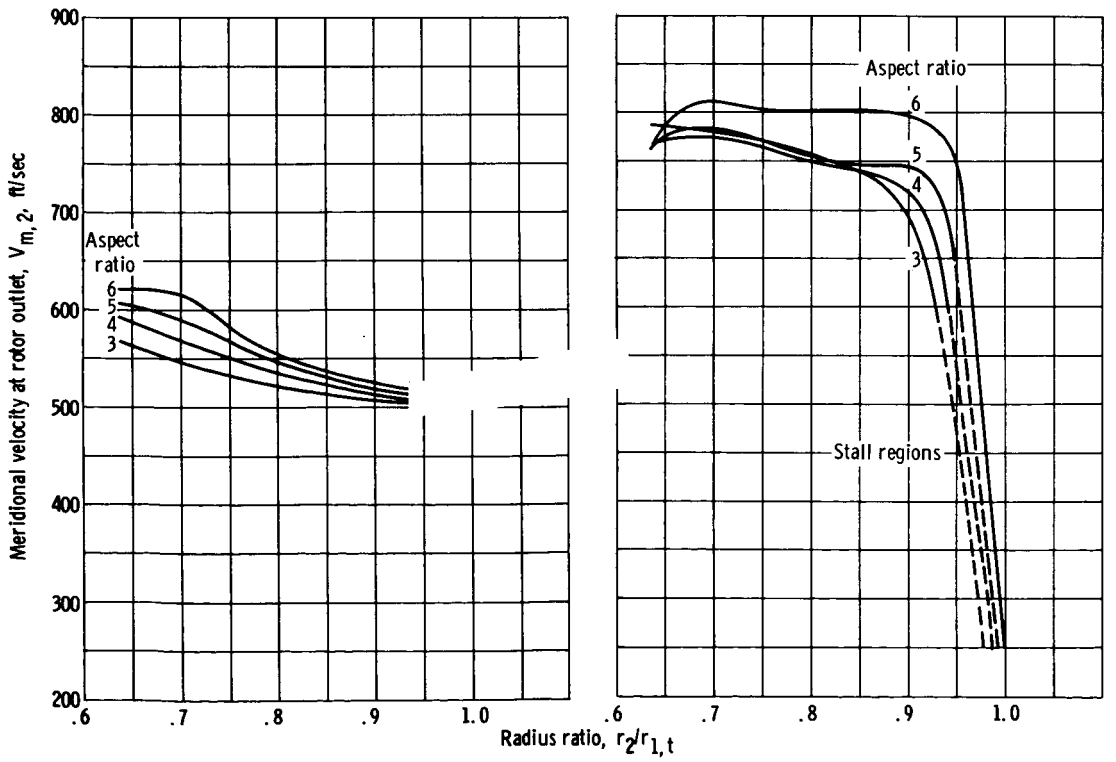

(e-1) Initial iteration - zero pressure losses. (e-2) Final iteration of pressure losses.

(e) Radial distribution of meridional velocity at rotor outlet.

Figure 2. - Continued.

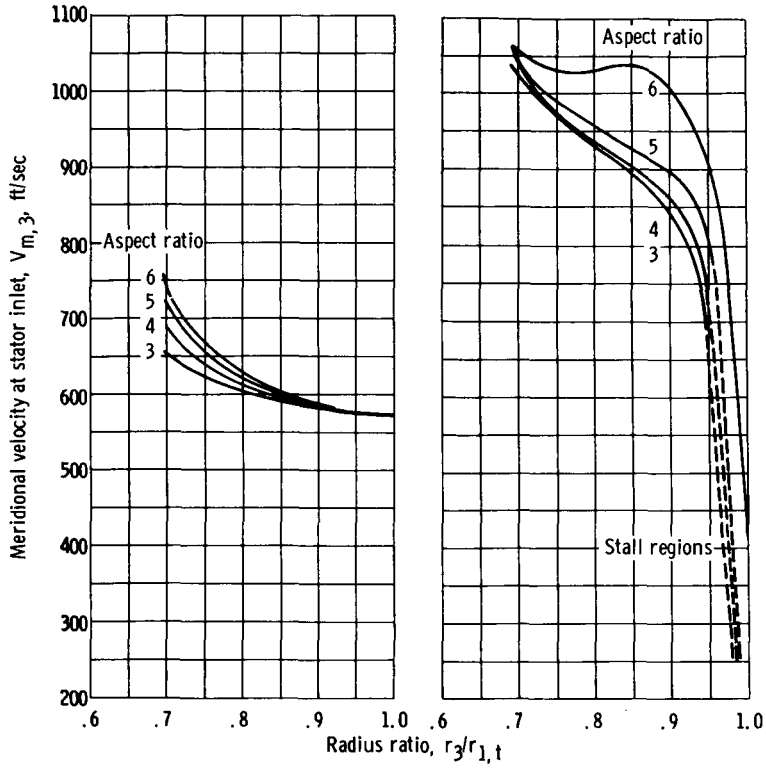

(f-1) Initial iteration - zero pressure losses.

(f-2) Final iteration of pressure losses.

(f) Radial distributions of meridional velocity at stator inlet.

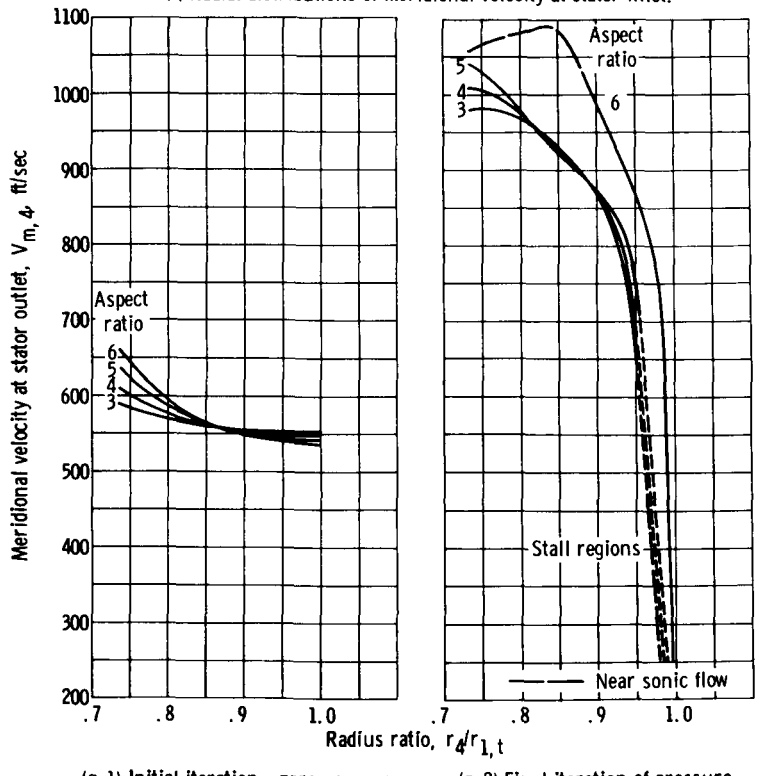

(g-1) Initial iteration - zero pressure losses.

(g-2) Final iteration of pressure losses.

(g) Radial distributions of meridional velocity at stator outlet.

Figure 2. - Continued.

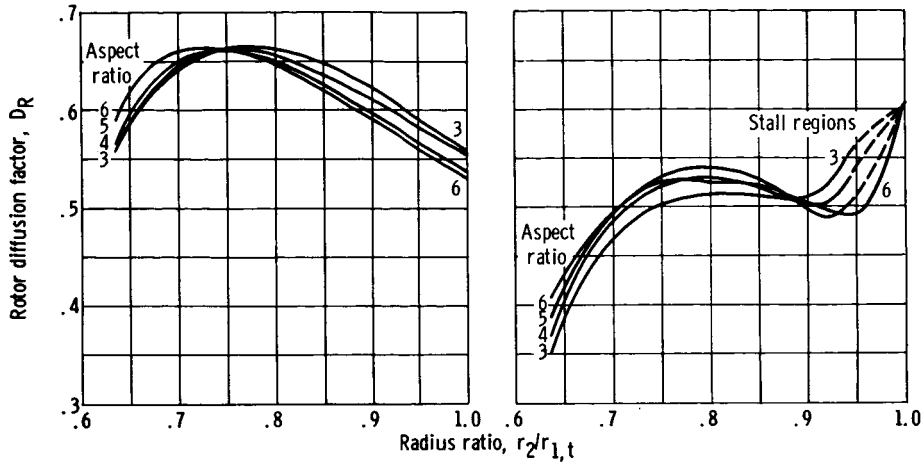

(h-1) Initial iteration - zero pressure losses. (h-2) Final iteration of pressure losses.

(h) Radial distributions of rotor diffusion factor.

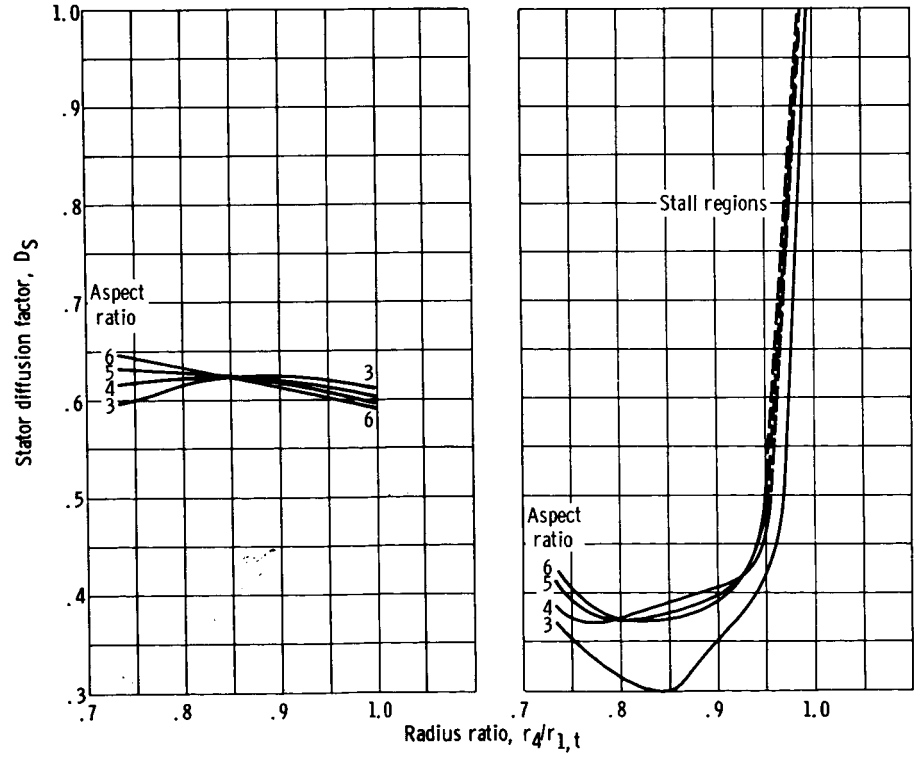

(i-1) Initial iteration - zero pressure losses. (i-2) Final iteration of pressure losses.

(i) Radial distribution of stator diffusion factor.

Figure 2. - Continued.

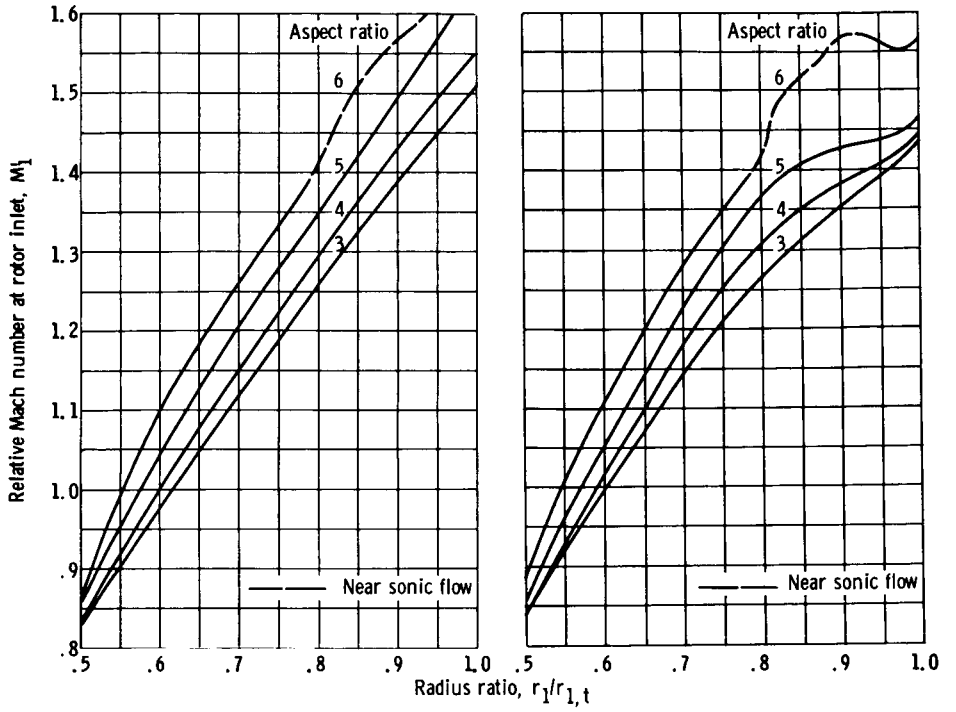

(j-1) Initial iteration - zero pressure losses. (j-2) Final iteration of pressure losses.

(j) Radial distribution of relative Mach number at rotor inlet.

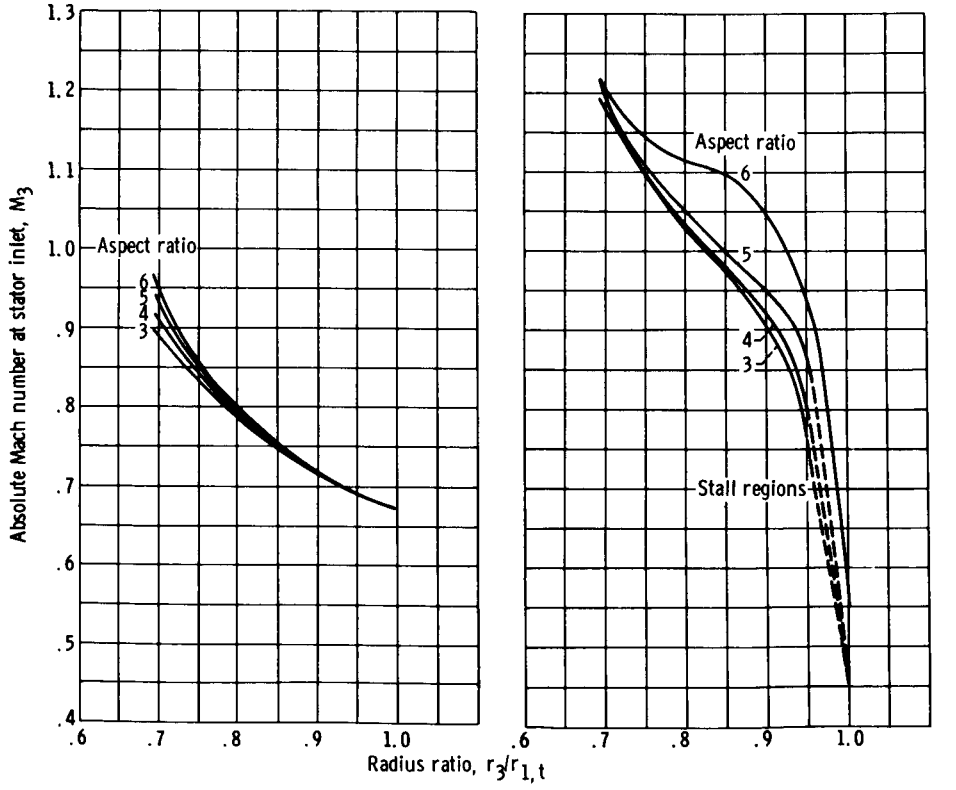

(k-1) Initial iteration - zero pressure losses. (k-2) Final iteration of pressure losses.

(k) Radial distributions of absolute Mach number at stator inlet.

Figure 2. - Continued.

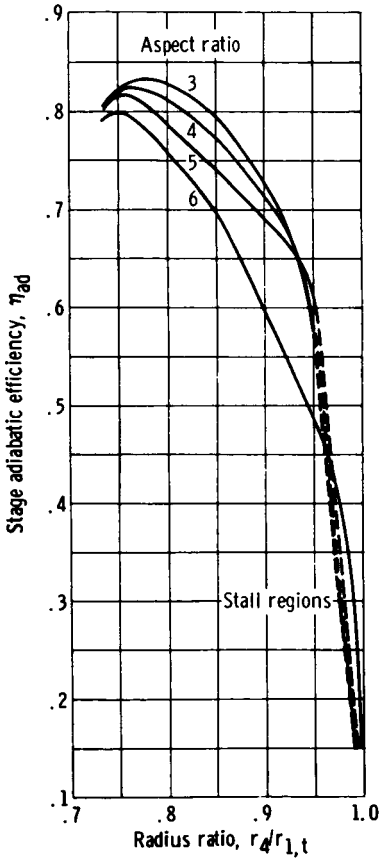

(l) Radial distributions of stage adiabatic efficiency for final iteration of pressure losses.

Figure 2. - Concluded.

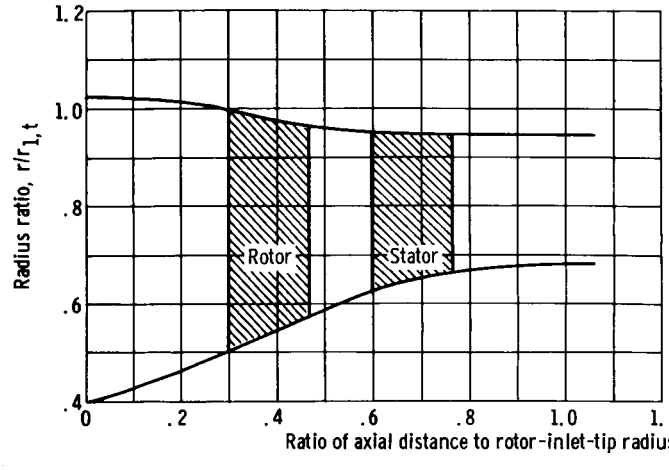

(a-1) Aspect ratio, 3.0.

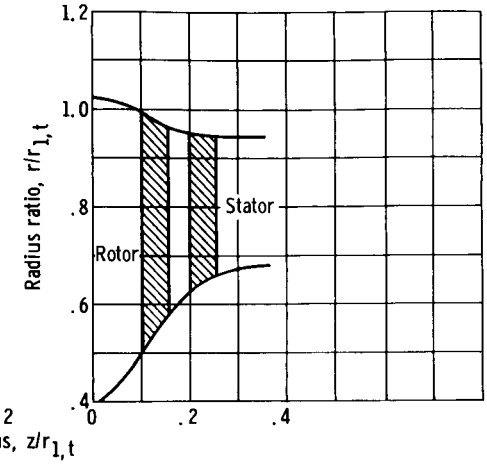

(a-2) Aspect ratio, 9.0.

(a) Typical geometry of compressor stages.

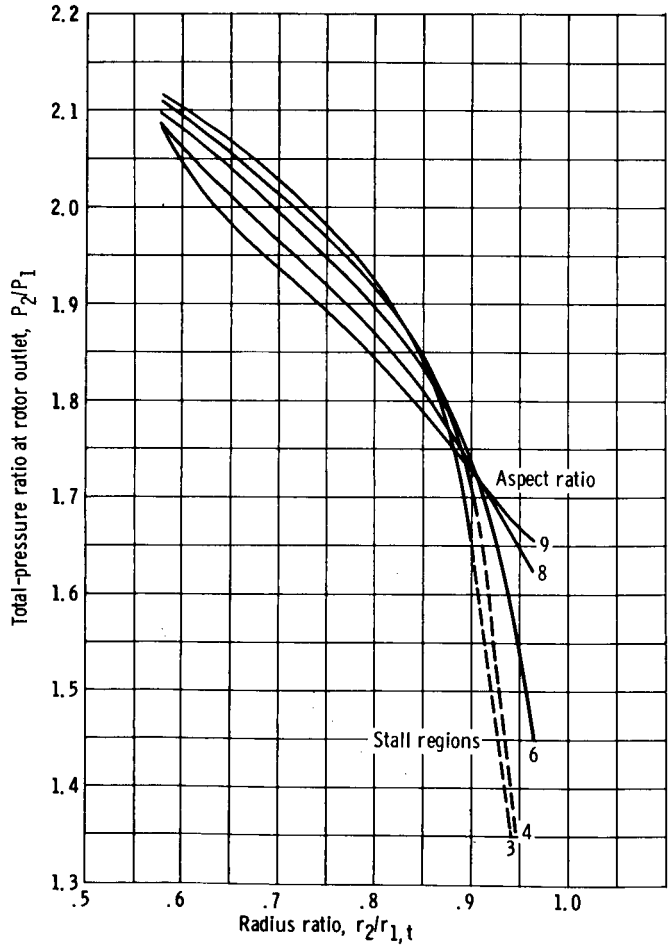

(b) Radial distributions of total pressure ratio at rotor outlet for final iteration of pressure losses.

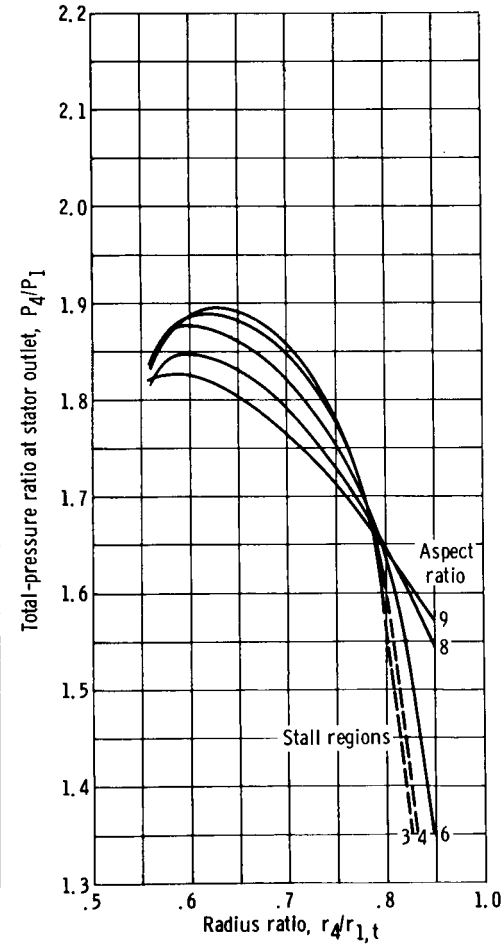

(c) Radial distributions of total pressure ratio at stator outlet for final iteration of pressure losses.

Figure 3. - Phase II studies of high-hub- and high-tip-curvature compressor stages for aspect ratios 3.0 to 9.0.

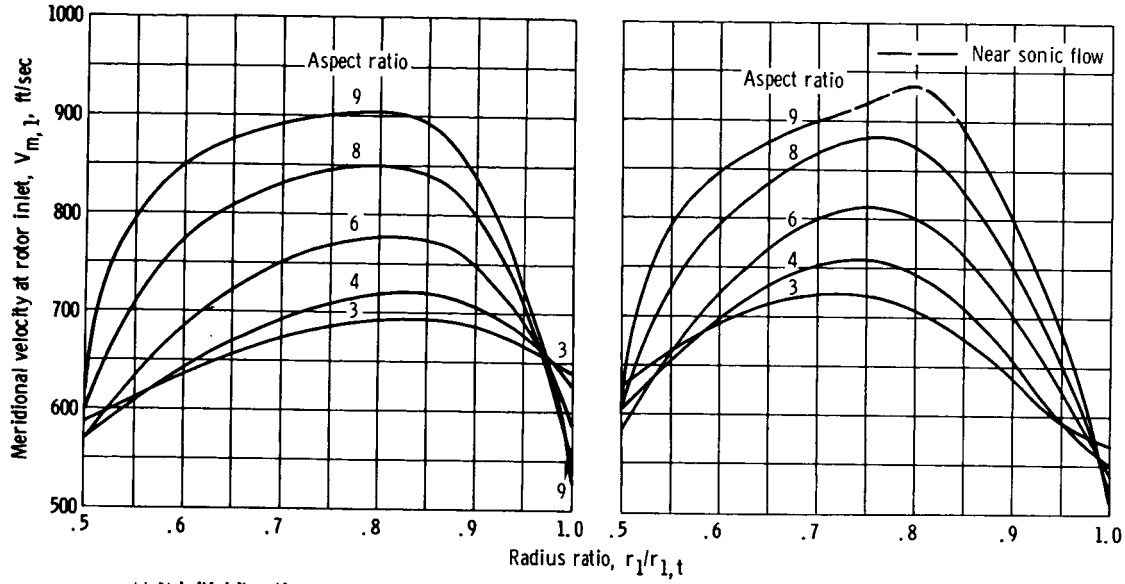

(d-1) Initial iteration - zero pressure losses. (d-2) Final iteration of pressure losses.

(d) Radial distributions of meridional velocity at rotor inlet.

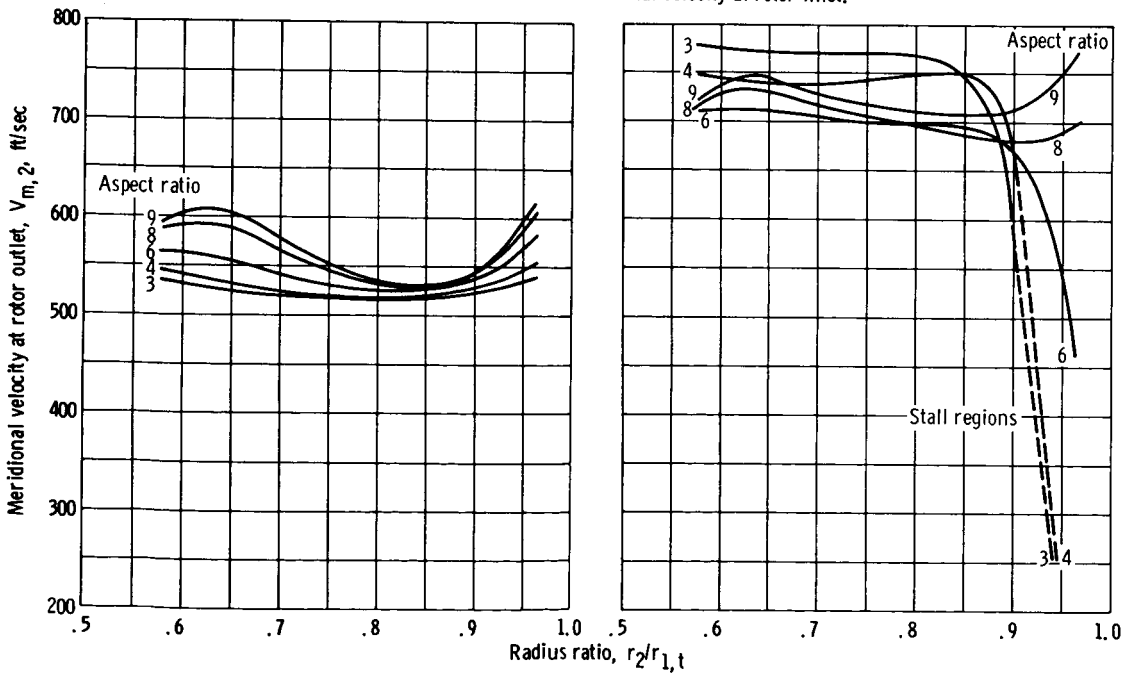

(e-1) Initial iteration - zero pressure losses. (e-2) Final iteration of pressure losses.

(e) Radial distributions of meridional velocity at rotor outlet.

Figure 3. - Continued.

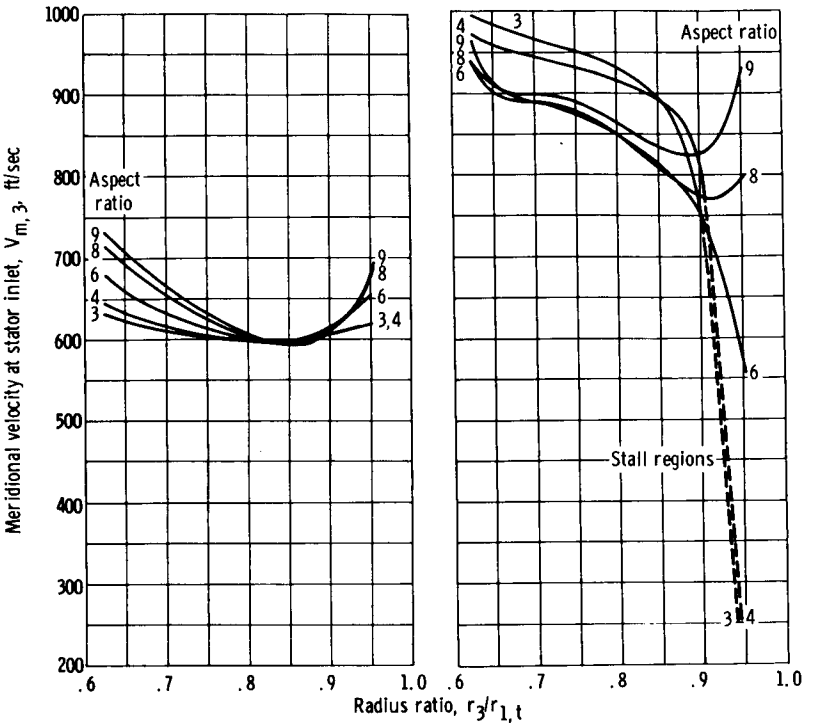

(f-1) Initial iteration - zero pressure losses.

(f-2) Final iteration of pressure losses.

(f) Radial distributions of meridional velocity at stator inlet.

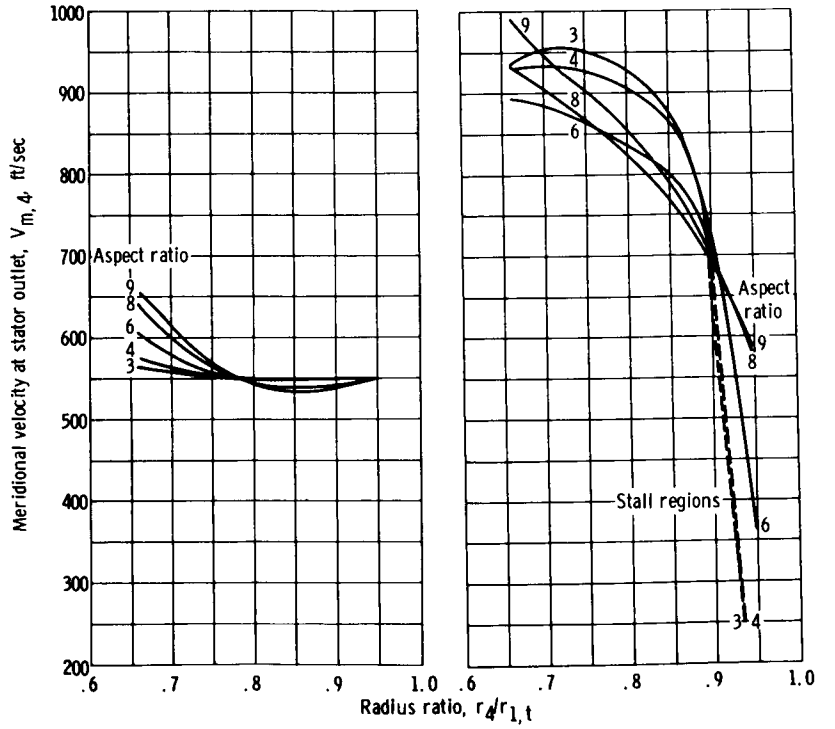

(g-1) Initial iteration of zero pressure losses.

(g-2) Final iteration of pressure losses.

(g) Radial distributions of meridional velocity at stator outlet.

Figure 3. - Continued.

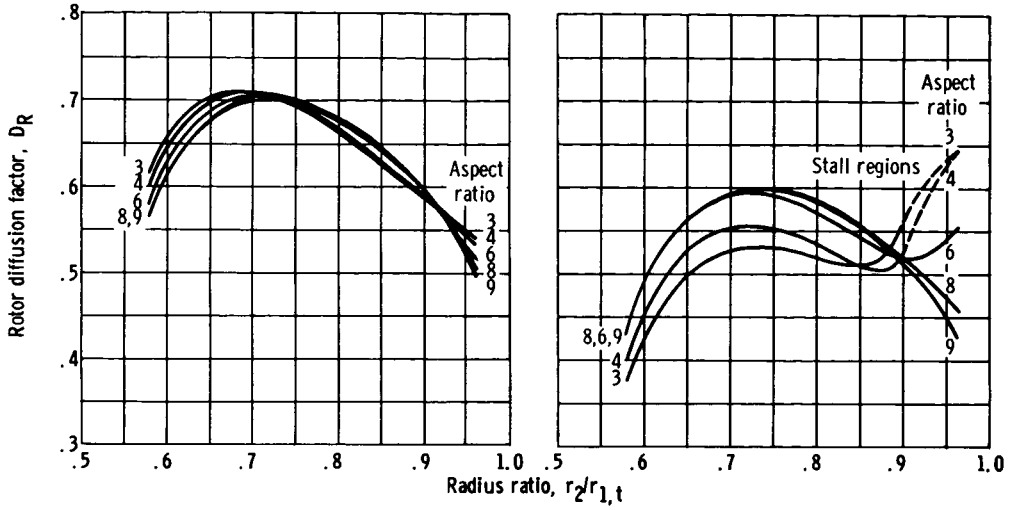

(h-1) Initial iteration - zero pressure losses. (h-2) Final iteration of pressure losses.

(h) Radial distribution of rotor diffusion factor.

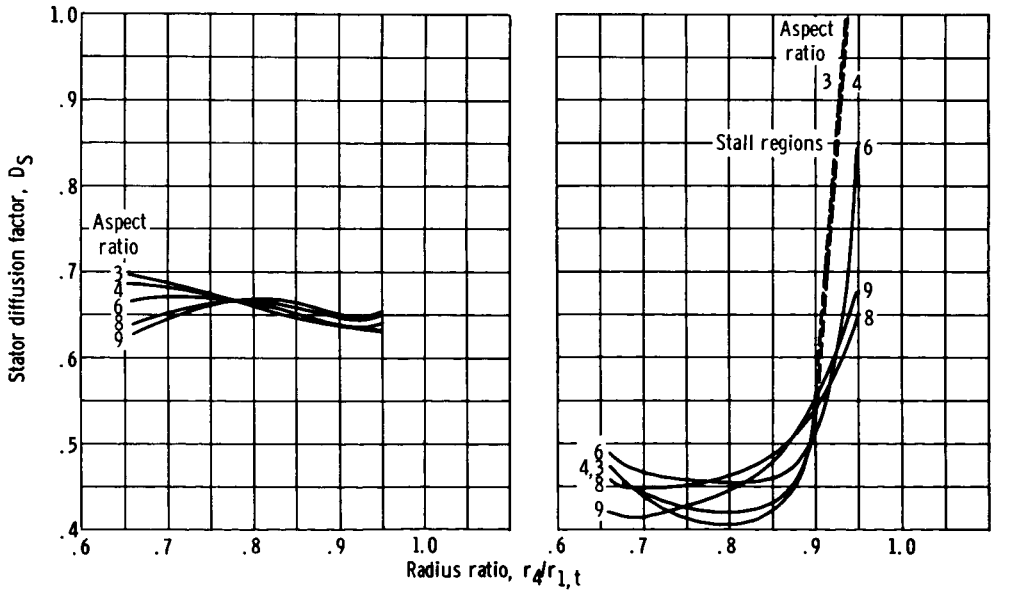

(i-1) Initial iteration - zero pressure losses. (i-2) Final iteration of pressure losses.

(i) Radial distributions of stator diffusion factor.

Figure 3. - Continued.

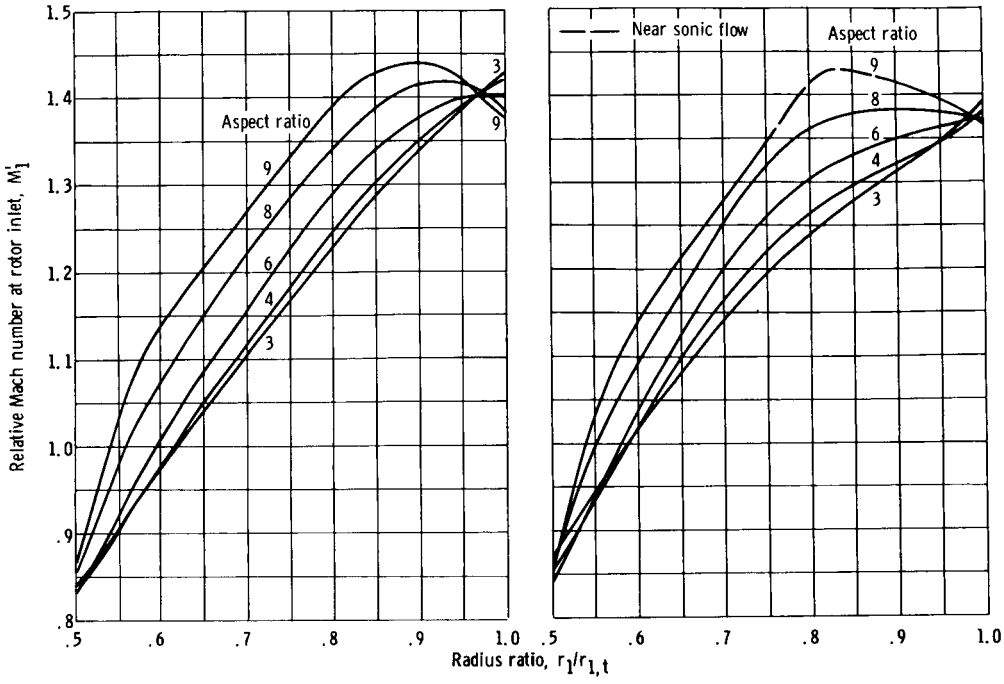

(j-1) Initial iteration - zero pressure losses. (j-2) Final iteration of pressure losses.

(j) Radial distributions of relative Mach number at rotor inlet.

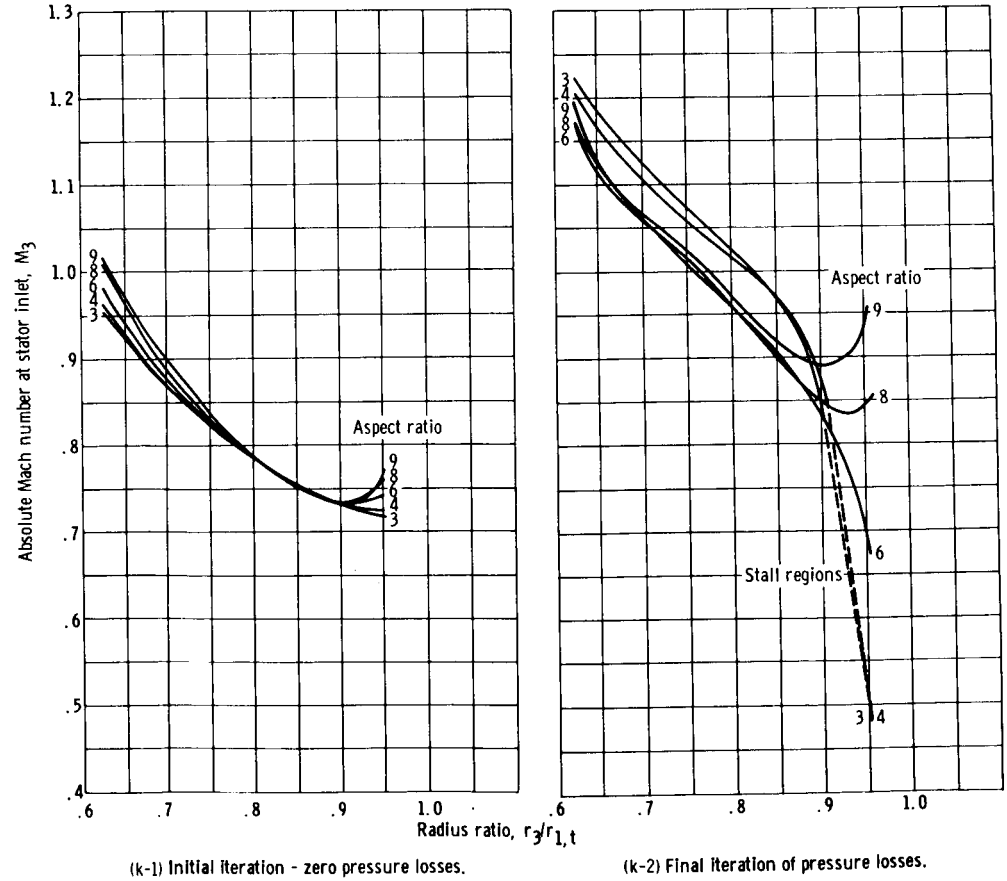

(k-1) Initial iteration - zero pressure losses. (k-2) Final iteration of pressure losses.

(k) Radial distributions of absolute Mach number at stator inlet.

Figure 3. - Continued.

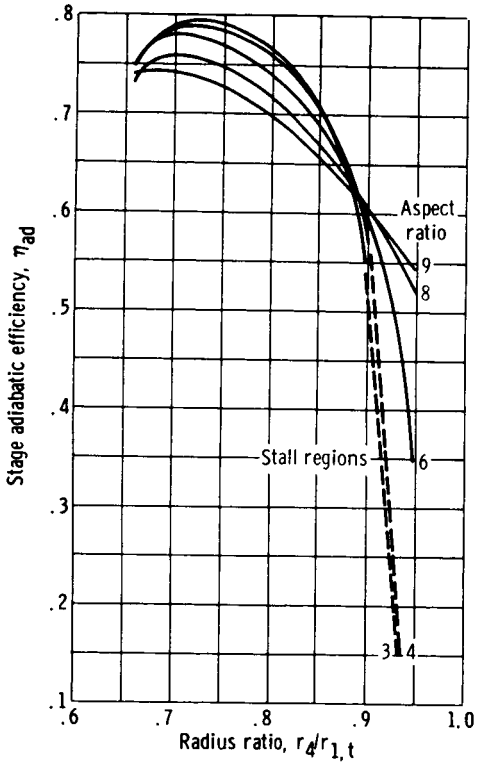

(l) Radial distributions of stage adiabatic efficiency for final iteration of pressure losses.

Figure 3. - Concluded.

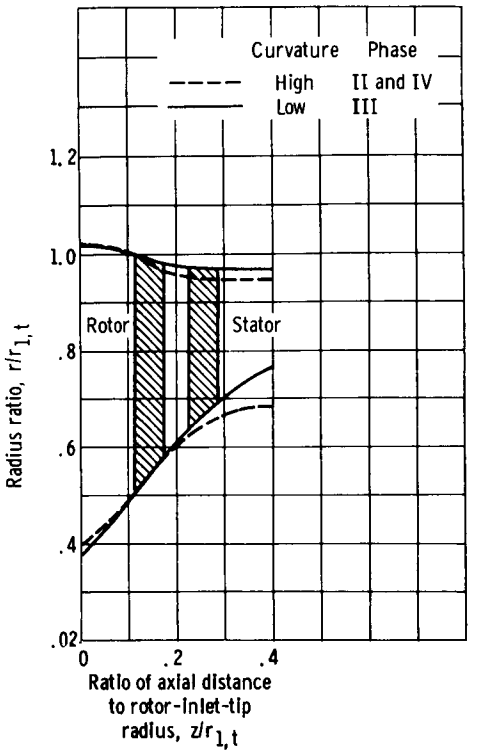

(a) Geometry of compressor stages.

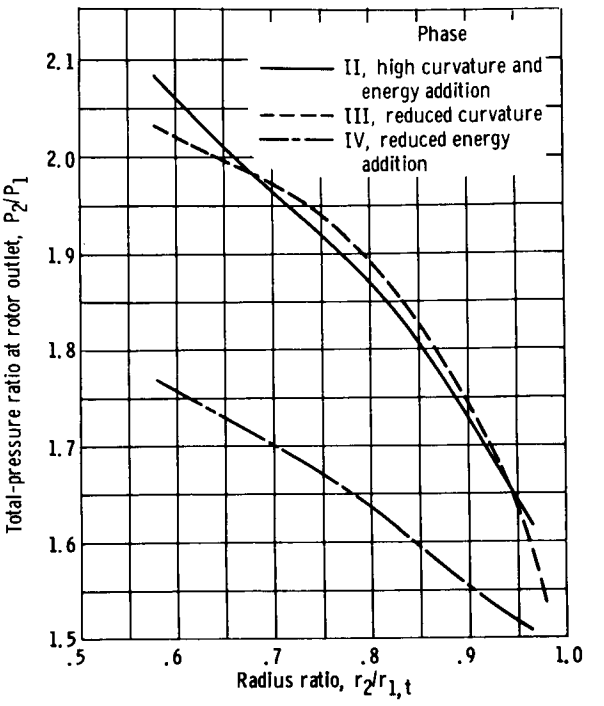

(b) Radial distributions of total-pressure ratio at rotor outlet.

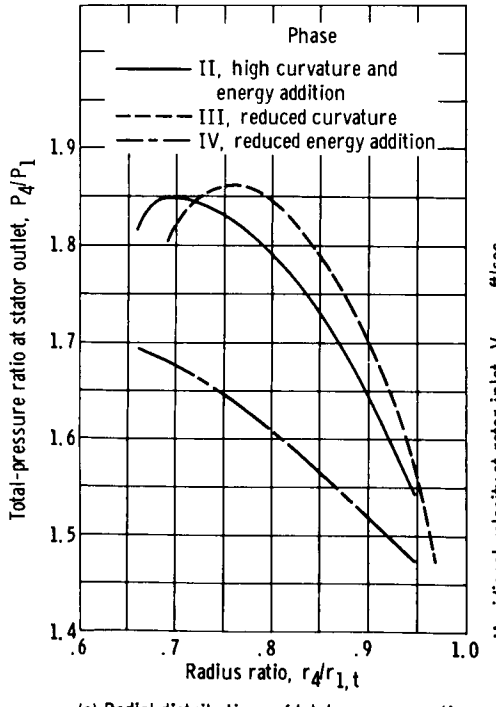

(c) Radial distributions of total-pressure ratio at stator outlet.

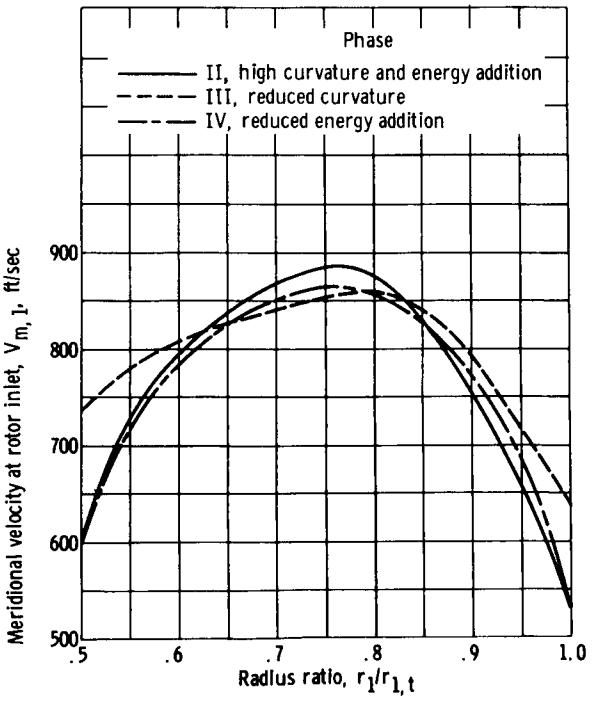

(d) Radial distributions of meridional velocity at rotor inlet.

Figure 4. - Phase II, III, and IV studies of 8.0-aspect-ratio compressor stages for final iterations of pressure losses.

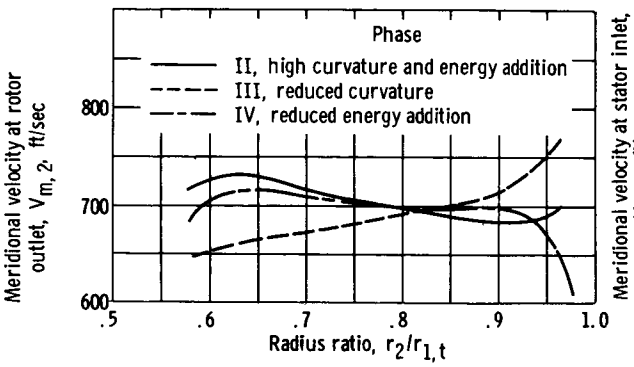

(e) Radial distributions of meridional velocity at rotor outlet.

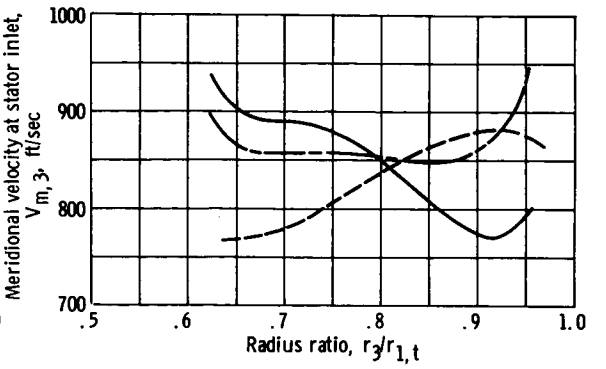

(f) Radial distributions of meridional velocity at stator inlet.

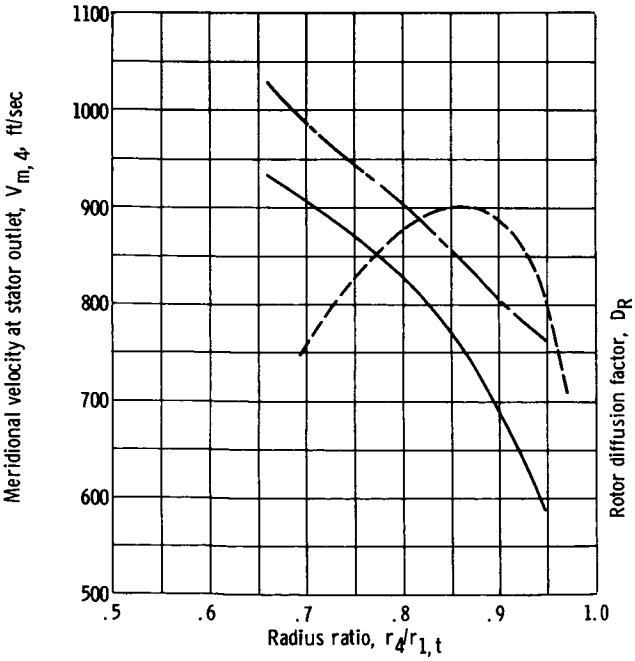

(g) Radial distributions of meridional velocity at stator outlet.

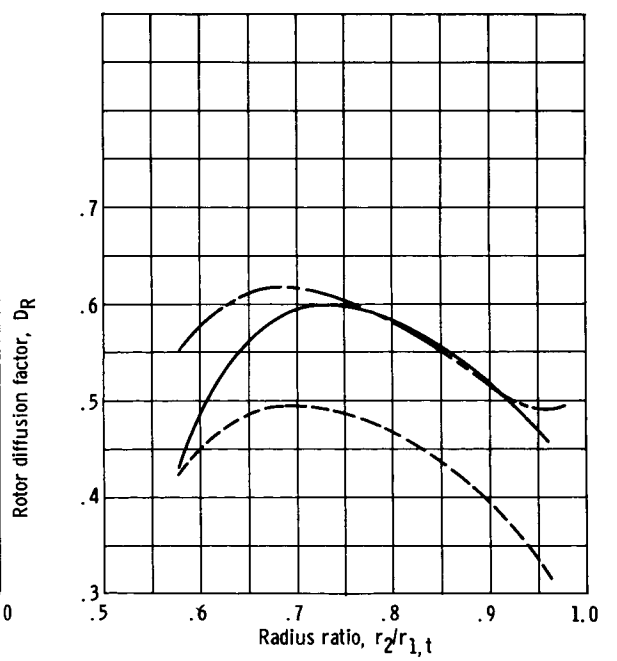

(h) Radial distributions of rotor diffusion factor.

Figure 4. - Continued.

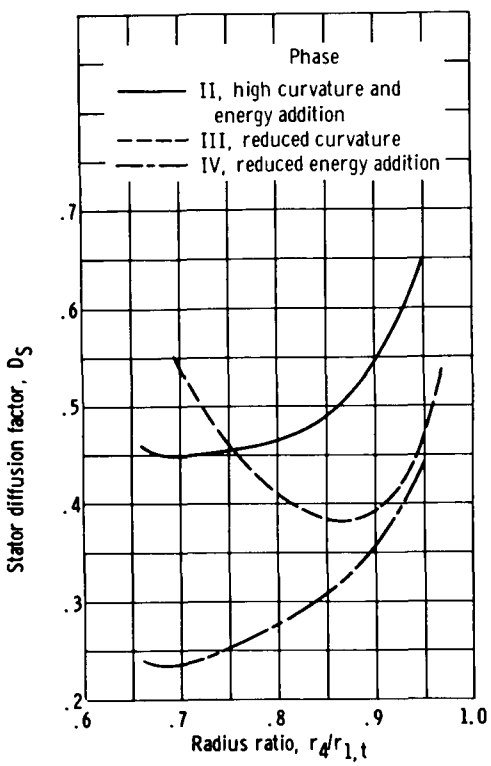

(i) Radial distributions of stator diffusion factor.

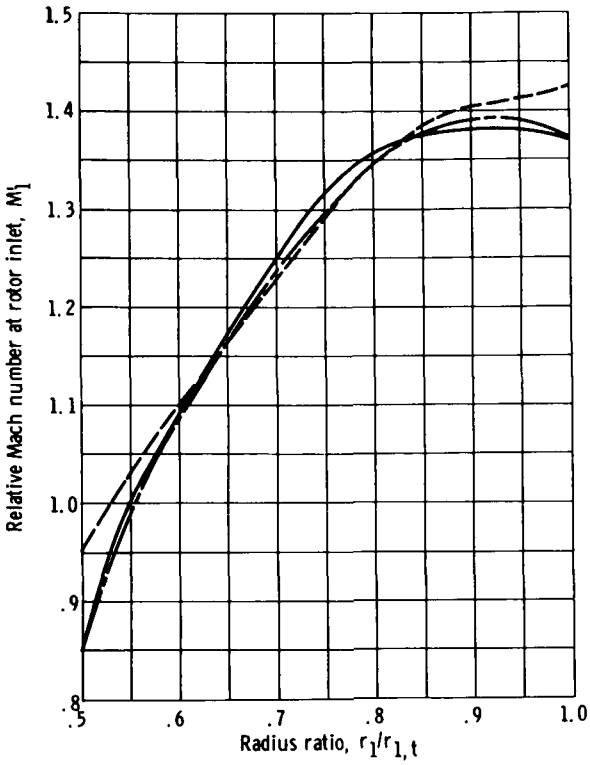

(j) Radial distributions of relative Mach number at rotor inlet.

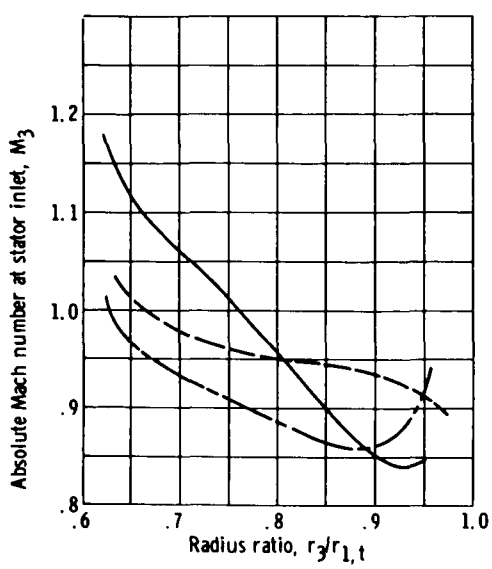

(k) Radial distributions of absolute Mach number at stator inlet.

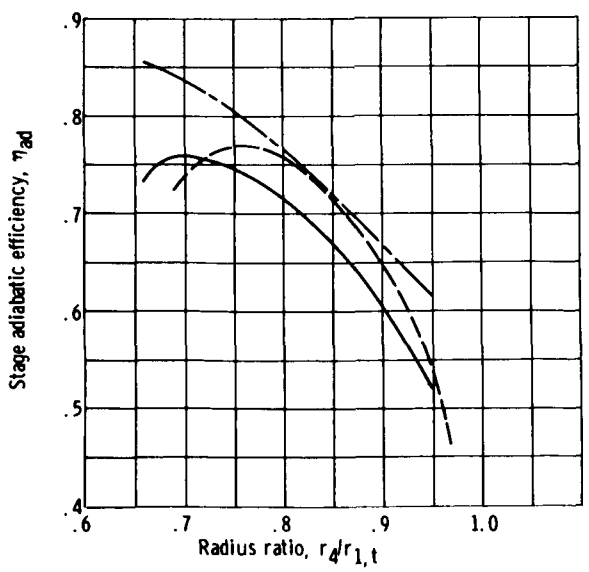

(l) Radial distributions of stage adiabatic efficiency.

Figure 4. - Concluded.

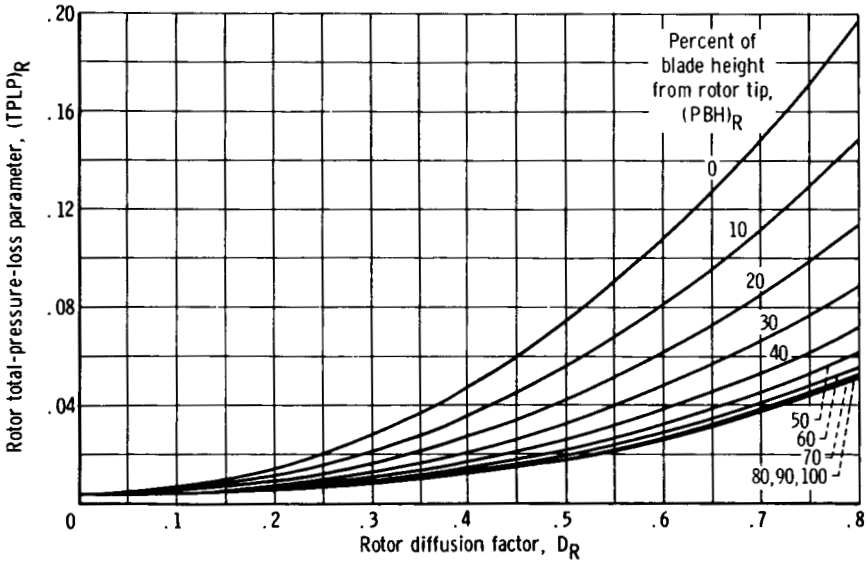

Figure 5. - Rotor total-pressure-loss parameter as function of diffusion factor and percent of blade height from tip (see eq. (B3)).

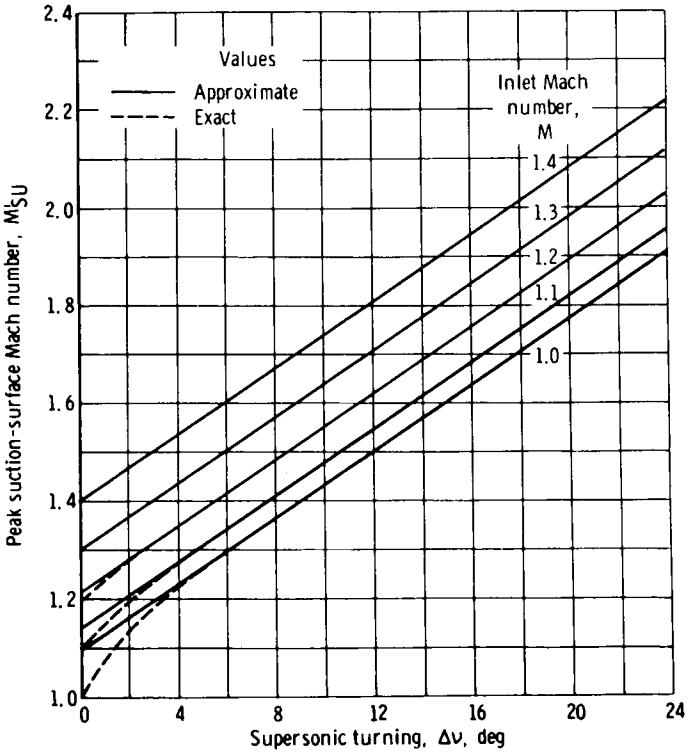

Figure 6. - Peak suction-surface Mach number as function of supersonic turning and inlet Mach number (see eq. (B7)).

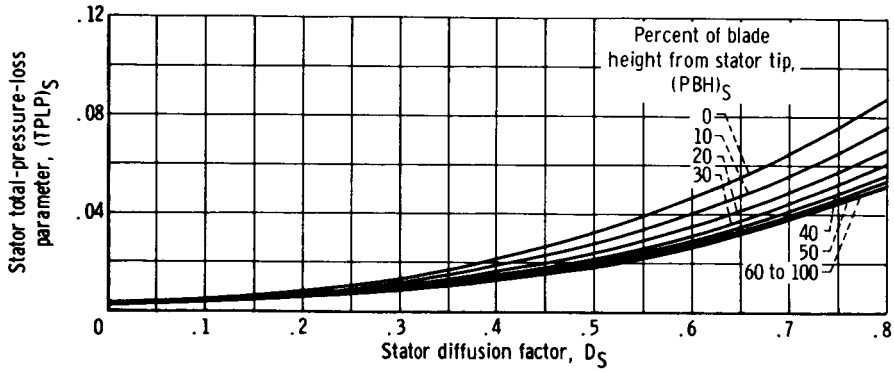

Figure 7. - Stator total-pressure-loss parameter as function of diffusion factor and percent of blade height from tip (see eq. (B18)).

9/5/67

"The aeronautical and space activities of the United States shall be conducted so as to contribute . . . to the expansion of human knowledge of phenomena in the atmosphere and space. The Administration shall provide for the widest practicable and appropriate dissemination of information concerning its activities and the results thereof."

—NATIONAL AERONAUTICS AND SPACE ACT OF 1958

NASA SCIENTIFIC AND TECHNICAL PUBLICATIONS

TECHNICAL REPORTS: Scientific and technical information considered important, complete, and a lasting contribution to existing knowledge.

TECHNICAL NOTES: Information less broad in scope but nevertheless of importance as a contribution to existing knowledge.

TECHNICAL MEMORANDUMS: Information receiving limited distribution because of preliminary data, security classification, or other reasons.

CONTRACTOR REPORTS: Scientific and technical information generated under a NASA contract or grant and considered an important contribution to existing knowledge.

TECHNICAL TRANSLATIONS: Information published in a foreign language considered to merit NASA distribution in English.

SPECIAL PUBLICATIONS: Information derived from or of value to NASA activities. Publications include conference proceedings, monographs, data compilations, handbooks, sourcebooks, and special bibliographies.

TECHNOLOGY UTILIZATION PUBLICATIONS: Information on technology used by NASA that may be of particular interest in commercial and other non-aerospace applications. Publications include Tech Briefs, Technology Utilization Reports and Notes, and Technology Surveys.

Details on the availability of these publications may be obtained from:

SCIENTIFIC AND TECHNICAL INFORMATION DIVISION

NATIONAL AERONAUTICS AND SPACE ADMINISTRATION

Washington, D.C. 20546